QA: NA

October 2001

Thermal Test Progress Report #7

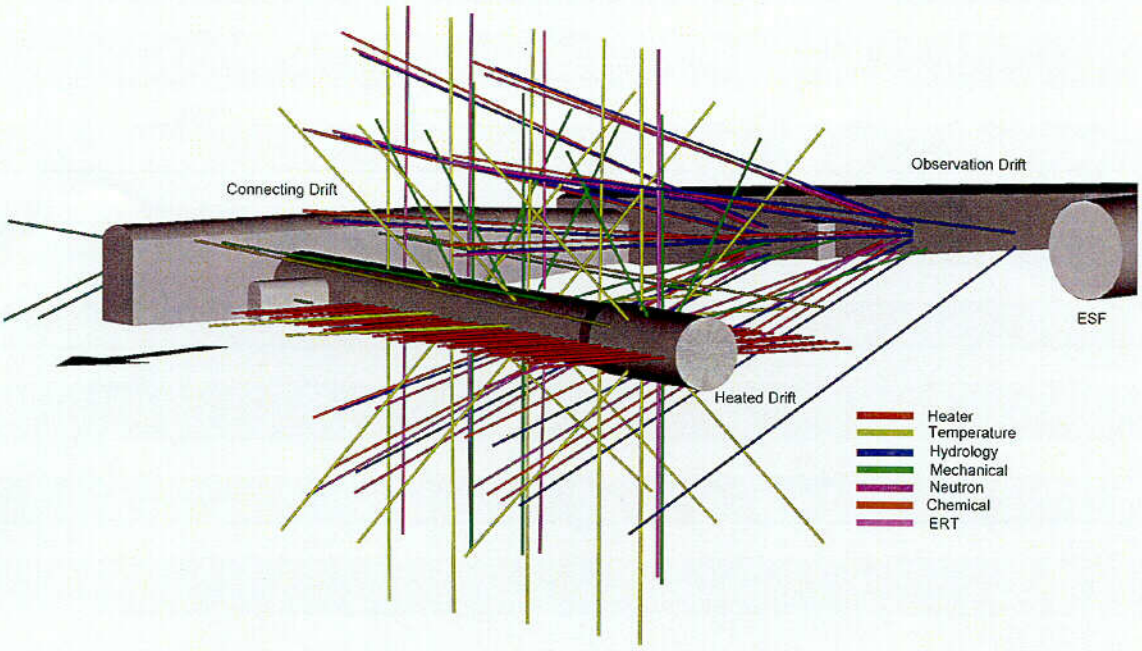

Prepared for:
U.S. Department of Energy
Yucca Mountain Site Characterization Office
P.O. Box 30307
North Las Vegas, Nevada 89036-0307

Prepared by:
Bechtel SAIC Company, LLC
1180 Town Center Drive
Las Vegas, Nevada 89144

Under Contract Number
DE-AC08-01NV12101

DRAFT DISCLAIMER

This contractor document was prepared for the U.S. Department of Energy (DOE), but has not undergone programmatic, policy, or publication review, and is provided for information only. The document provides preliminary information that may change based on new information or analysis, and is not intended for publication or wide distribution; it is a lower level contractor document that may or may not directly contribute to a published DOE report. Although this document has undergone technical reviews at the contractor organization, it has not undergone a DOE policy review. Therefore, the views and opinions of authors expressed do not necessarily state or reflect those of the DOE. However, in the interest of the rapid transfer of information, we are providing this document for your information, per your request.

QA: NA

October 2001

Thermal Test Progress Report #7

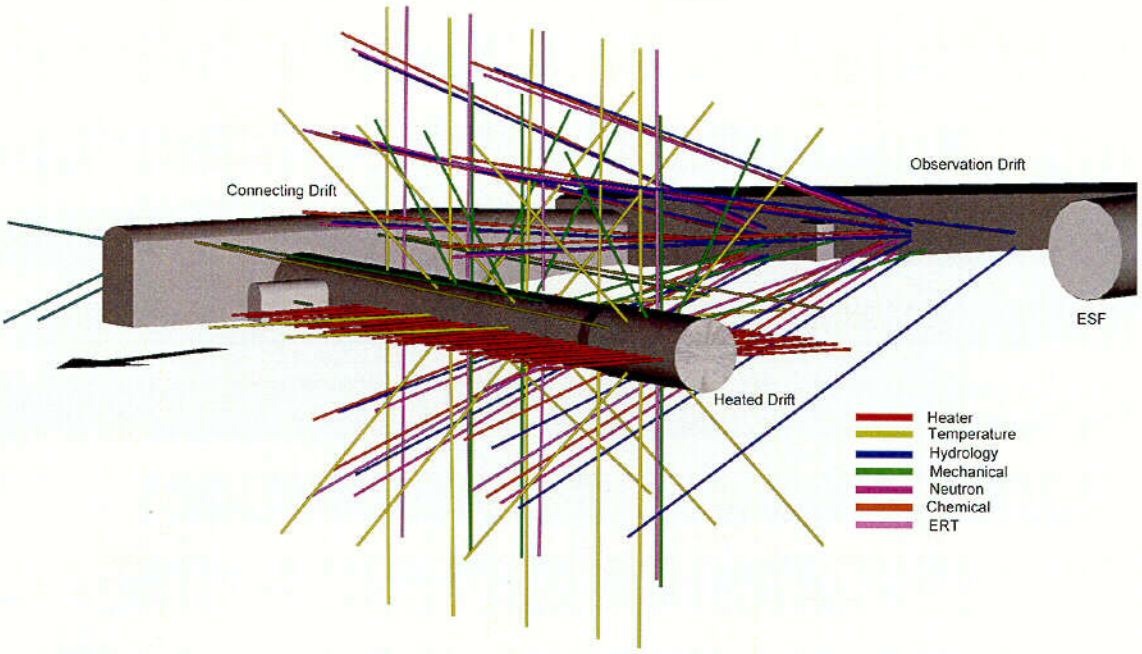

Prepared for:
U.S. Department of Energy
Yucca Mountain Site Characterization Office
P.O. Box 30307
North Las Vegas, Nevada 89036-0307

Prepared by:
Bechtel SAIC Company, LLC
1180 Town Center Drive
Las Vegas, Nevada 89144

Under Contract Number
DE-AC08-01NV12101

C02

INTENTIONALLY LEFT BLANK

CONTENTS

INTENTIONALLY LEFT BLANK

1. INTRODUCTION

This Thermal Test Progress Report #7 is the seventh in the series of informal reports intended to communicate the progress of the Yucca Mountain Project (YMP) thermal test program. This report consists of diverse thermal related topics including those discussed at the last thermal test workshop held at YMP Summerlin facilities in Las Vegas in June 2001. The Large Block Test and Single Heater Test are complete so most of the discussion in this progress report relates to the Drift Scale Test (DST). Planning is now underway for the Cross Drift Thermal Test. Some additional material on thermal testing available at the time of publication and relevant to the progress of the thermal tests is included.

This progress report is mostly a compilation of individual works that may contain speculation and conclusions that do not necessarily reflect a consensus within the thermal test team. These progress reports are intended to informally communicate the progress of the in-situ thermal tests and should be considered preliminary in nature.

This report is generally organized where chapters represents processes, coupled processes, or some other major subpart of the thermal test work. Sections within each chapter represent individual contributions.

As in previous reports authors and contributors are not specifically recognized. The thermal test team includes members from the Integrated Science Solutions, Inc., Lawrence Berkeley National Laboratory, Lawrence Livermore National Laboratory, Los Alamos national Laboratory, Sandia National Laboratory, U. S. Geological Survey, and the Department of Energy.

Appendix A contains index figures of the Drift Scale Test layout, borehole configurations, and other general information. There are two common location referencing frameworks. A local coordinate system has been established for each of the thermal tests to date. This is shown in Appendix A for the DST. Another common data reporting method uses the distance along a borehole as measured from the collar or the borehole. A table of borehole locations is included in Appendix A. Boreholes may be referenced by one of two unique names: the borehole number or their functional sequence number.

INTENTIONALLY LEFT BLANK

2. GENERAL TOPICS

This chapter includes discussion of two general topics relating to the Drift Scale Test (DST). Sections 2.1 and 2.2 relate to scaling along the roof of the heated drift and include the white paper and a description of follow-up camera examination of the heated drift. A proposed Thermal Test Measurement Report is described in Section 2.3.

2.1 Drift Scale Test White Paper: Scaling Along the Roof of the Heated Drift

Conclusions

The occurrence of limited scaling from four small zones along the roof of the Heated Drift of the Drift Scale Test (DST) is not surprising. The middle nonlithophysal rock (Tptpmn) is highly fractured, and additional fractures were likely created during the drift construction process. This altered zone around the drift, especially above the Heated Drift, is also exacerbated by:

- aggressive heating that is estimated to be 6 and 12 times the areal thermal loading associated with the EDA-II and alternative low-temperature designs, respectively.
- potential for transient thermal stresses to exceed rock strength especially along the rough surface of the roof of the Heated Drift where stress concentrations can be high, maximum temperature increases are approximately 180 ^{0}C, and the rock is not well confined.
- proximity of instrumentation and rockbolt holes to the observed scaling zones.

The addition of heat increases the circumferential stresses around the Heated Drift creating conditions that would lead to some small amounts of rock scaling from the roof. The fallen rocks appear to be shaped like flat plates which is consistent with the development of circumferential fractures by a thermally induced biaxial stress state.

The amount of fallen rock observed is relatively small which would indicate that rock damage is superficial. This conclusion is further supported by mechanical (MPBX) measurements that do not indicate large-scale, deeply penetrating rock movements that suggest effects of scaling are limited to the surface of the Heated Drift.

The existing ground support system comprised of rockbolts and welded wire fabric continues to perform as designed. Despite the appearance of inelastic deformation, onsite personnel with much experience assessing ground support systems believe the welded wire fabric and rockbolts remain competent and will continue to support the existing loose rock in the observed scaling zones.

Given the superficial nature of the observed scaling zones, adverse consequences of these scaling zones are expected to minimally impact the performance of the Drift Scale Test. To date, test equipment, instrumentation, and sensors have not been damaged and it appears the DST will complete its planned four-year heating duration in December 2001. The heating phase is planned to be followed by a cooling phase of similar duration.

Ground support of rockbolts and welded wire fabric has functioned as expected for controlling and containing this type of rock behavior. The occurrence of the observed scaling zones is consistent with conceptual understanding of the thermal-mechanical behavior of the rock mass involving pre-closure and post-closure performance of the potential repository.

Background

The DST is a large scale, heated field test designed to generate and to observe thermally-driven effects on hydrological, mechanical, and chemical processes in the welded tuff units of the potential repository at Yucca Mountain. The specific evolution of the DST will not directly mimic the potential repository, but the same processes will occur, be quantified, and allow validation of the Project models of such processes. The DST is densely instrumented to record temperatures, rock movement, fluid movement, gas flow, and to sample liquids and gases from the rock mass. The Drift Scale Test centers around a 47.5 m long Heated Drift that is 5 m in diameter.

As shown in the as-built report for the DST ("Drift Scale Test As-Built Report", BAB000000-01717-5700-00003), the Heated Drift is isolated from workers and visitors with a bulkhead to provide safety from the high temperatures and to isolate the test from external conditions. Nine floor/canister heaters in the Heated Drift and fifty wing heaters

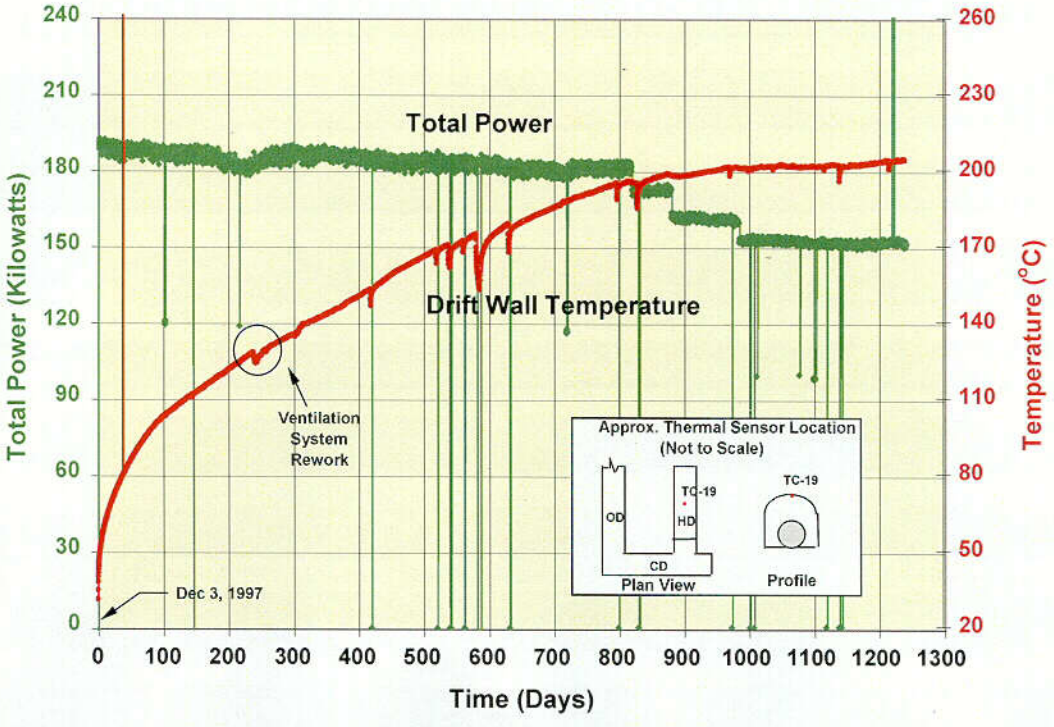

Figure 1. Power and Drift Wall Temperature Histories for the Drift Scale Test.

C03

BAB000000-01717-4600-00007). (in horizontal boreholes perpendicular to the drift) initially generated approximately 190 kW of power over a 1500 m^2 area ("Drift Scale Test Design and Forecast Results",

As shown in Figure 1, the test is almost three and one half years into the planned four-year heating period (Section 8 of the DST design report). Figure 1 also shows several unplanned power outages and three planned power reductions of 5 percent each. None of these power reductions appear to contribute to the development of the observed scaling zones because the timing is different and the decreases are small when compared to total outages. The planned thermal management strategy for the DST includes maintaining the wall temperature in the Heated Drift at approximately 200 °C. Although the wall temperatures vary especially at either end of the Heated Drift, most of the wall temperatures are near 200 °C because of the effectiveness of radiative heat transfer.

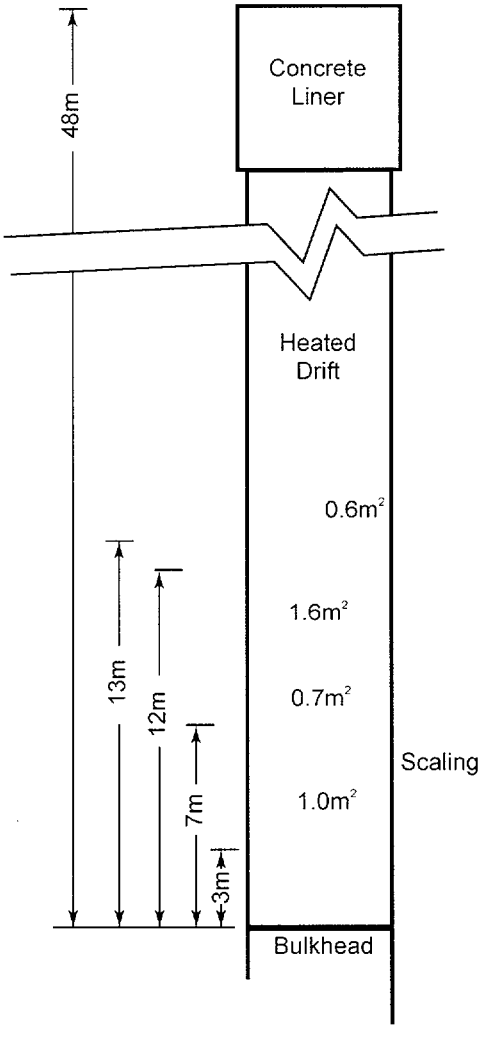

Figure 2. Plan view of the DST Heated Drift Showing Locations of Four Scaling Zones (Note: the lack of zones farther from the bulkhead reflect limitations on clear observations.).

The ground support system for the roof consists of rockbolts and welded wire fabric through the first 35 meters of the Heated Drift. The support system for the remaining 12.5 meters consists of a concrete liner, which covers the rockbolts and welded wire fabric, and extends to the far end of the Heated Drift (see Figure 2 and Figure 3 showing layout sketch and pre-test conditions, respectively).

Limited scaling has been observed in the roof of the Heated Drift in four zones, each covering an area less than two square meters. Associated with each of these scaling zones are small pieces of rock on the floor that have dropped through the 3-inch-by-3-inch openings in the welded wire fabric. These scaling zones have been contained by the existing ground support system in the manner it was designed. This recent scaling behavior is discussed herein in terms of observations, analyses, future activities, and conclusions.

Figure 3. View of the Drift Scale Test Prior to Heater Activation (Note: several distinct ridges along the roof of the Heated Drift which appear to coincide with observed scaling zones).

Observations

Early visual observations documented by e-mail dated November 16, 1999 (Doug Weaver to Mark Peters) indicated the presence of small rock chips on the floor located 5 to 20 m from the bulkhead. This observation triggered further investigation with the DST remote camera. Although small rock chips were present on the floor, there was no evidence of accumulated larger rock fragments retained in the welded wire fabric.

During a recent cleaning and re-installation of the DST bulkhead windows (April 23, 2001), loose rock was observed at several locations above the welded wire fabric attached to the roof of the Heated Drift. Observations were conducted by Agustin Passalacqua

C04

(Title III Engineer), Doug Weaver (Test Coordination Office), and Keith Dennison (Underground Mining Foreman). Cables from two instrumented boreholes located 2.7 m and 11.9 m from the bulkhead along the longitudinal axis of the Heated Drift were observed to have pulled loose from the welded wire fabric. These cables were originally fastened to the wire fabric during installation and remained fastened during prior video imaging in October 2000. This suggests that much of the scaling had occurred since then. To better characterize the extent of the loose rock, remote video imaging of the inside of the Heated Drift was scheduled for the following week.

On May 2, 2001, the extent of scaling along the roof of the Heated Drift was further examined by Doug Weaver (Test Coordination Office), Agustin Passalacqua (Title III Engineer), Dan Neubauer (Test Coordination Office), Dave Wehner (Photo Services), Robert Jones (NFE Integration/Implementation), and Gene Griego (TCO Field Rep). Video images were recorded with the DST's remote video camera and with an additional video unit mounted at the bulkhead. In addition, photographs were taken with a 35mm camera with a telephoto lens. The 7.5 cm squares in the welded wire fabric provide a usable reference scale in the images.

At 8:20 AM (May 2, 2001), the camera door was opened and the video equipment prepared. The insulated camera box, that contains two video cameras, successfully traveled the full length of the rail mounted to the roof of the Heated Drift (see Figure 4). One of the cameras recorded roof, wall, and floor images by rotating the lens about the longitudinal axis of the Heated Drift. However, this camera did not image most of the scaling zones because the camera's blind spot created by rotational limitations of 320° does not allow it to view that part of the roof. The second remote camera is forward looking. It was not intended to record images along the roof of the Heated Drift.

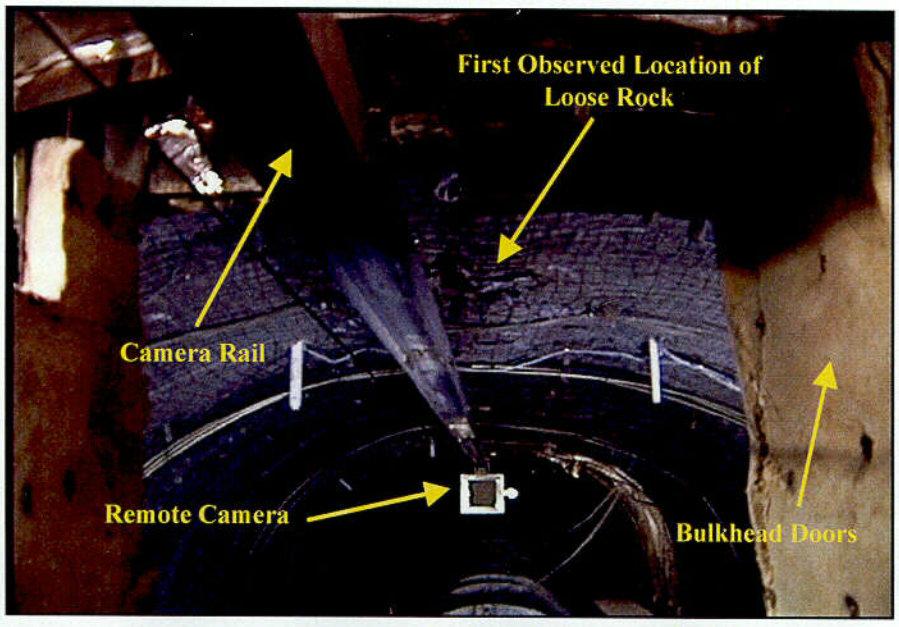

Figure 4. View From DST Bulkhead Doors for Remote Camera Looking Into the Heated Drift. (Note: loose rock is 3 m from the bulkhead and welded wire fabric consists of 7.5 cm squares)

C05

At the far end of the Heated Drift (35 to 47.5 meters from the bulkhead), the drift periphery is covered with a concrete liner. The traveling remote camera clearly showed that this concrete liner remained intact with no evidence of fractures or damage from heating. Although these analog images are not available in digital electronic format, they can be obtained and viewed by contacting Doug Weaver (702-295-5916). The digital video of the drift is available as AVI files over the network (either by FTP or in the DST directory on the G-drive).

From the observations, sketches of the scaling zones along the roof were developed. Most of these observations were made from the viewing window located on the lower left side of the bulkhead. Figure 2 shows four zones of observed scaling that were mapped by estimating the number welded wire fabric squares that held loose rock. The three zones closest to the bulkhead showed scaling concentrated along the roof's crown (i.e., the apex). A forth zone was located about at the 2:00 o'clock position relative to the roof's crown, about 13 meters into the Heated Drift. For the scaling zone closest to the bulkhead (about 3 m from the bulkhead), the elongated area is estimated to be 1.0 m^2 (see Figure 5). The existing ground support system of rockbolts and welded wire fabric shown in Figure 5 continues to perform as designed. Despite the appearance of inelastic deformation, onsite personnel with much experience assessing ground support systems believe the welded wire fabric and rockbolts remain competent and will continue to support the existing loose rock in the observed scaling zones.

Figure 5. View of Scaling Located 3 m From the DST Bulkhead and Retained in the Ground Support System Comprised of Rockbolts and Welded Wire Fabric (Note: welded wire fabric consists of 7.5 cm squares)

C06

For the scaling zone located about 7 m from the bulkhead, the lens-shaped area is estimated to be 0.7 m^2. At 12.5 m from the bulkhead, a somewhat circular zone is estimated to cover an area of about 1.6 m^2. Located close to the collar or instrument head of a multi-point borehole extensometer referred to as MPBX-3, the fourth scaling zone covers an area of approximately 0.6 m^2 (see Photo 4). The loose rock fragments appear to have thickness between 2 to 5 cm. The ground support is expected to retain the scaling shown in Figure 6.

Other scaling zones may exist further from the bulkhead, however observation and characterization was hindered because of the distance and lighting constraints of these zones. Small chips of rock observed along the floor suggest that additional scaling zones exist. Even the characterization of the two scaling zones located at 12 m and 13 m from the bulkhead was difficult because of distance from the viewing window and poor illumination.

The ground support system, that was installed during the Heated Drift excavation approximately fours years ago, consists of 3 meter long Super Swellex rockbolts installed on a one meter square pattern and 3x3xW1.9xW1.9 welded wire fabric. This ground support was installed above the springline of the excavation. According to the field engineers, the welded wire fabric and rockbolt ground support system is functioning as designed. Also, there is not any evidence of failed components or deep fractures. Pieces of rock that were held by the welded wire fabric varied in diameter from about 5 cm (silver dollar size) to about 20 cm (dinner plate size). The loose rock fragments, which appear to be mostly flattened shapes, are indicative of rock scaling.

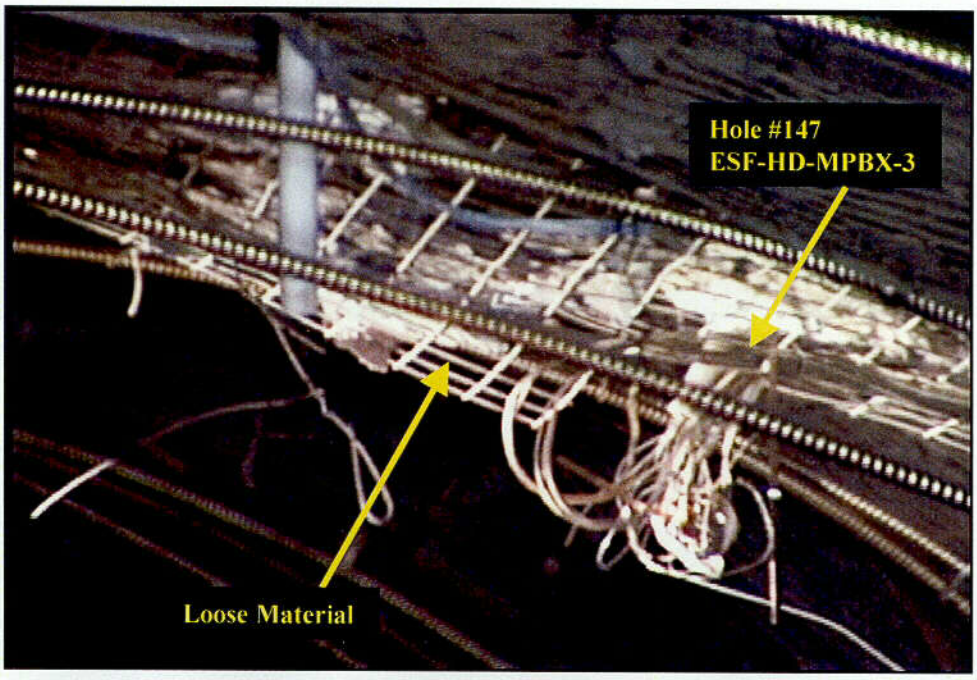

Figure 6. View of Scaling Located Approximately 13 m from the DST Bulkhead. (Note: loose rock appears close to the MPBX-3 instrument head and welded wire fabric consists of 7.5 cm squares.)

C07

In addition to the remote video run, the YMP project photographer set up digital video and still photography equipment on the door platform for the remote camera. From that vantage point, high-resolution images of the loose rocks held by the rockbolts and welded wire fabric at several of the zones described above were obtained. Photographs of the roof suggest most of the observed scaling zones are associated with uneven surfaces or ridges left by alpine mining machine during excavation of the Heated Drift. This observation is not surprising since these irregular ridges should experience higher stress concentrations and thus more failure than smoother surfaces along the drift periphery. Upon completion of the observations, the bulkhead remote camera doors were closed and taped shut at 10:06 AM.

Analyses

In addition to direct observations of the scaling zones, other information and data were analyzed to better characterize and assess the extent of the processes resulting in the loose rock behind the welded wire fabric in the DST Heated Drift.

Pre-Test Fracture Mapping

The pretest fracture map of the periphery of the Heated Drift (Section 7 of the report entitled "Ambient Characterization of the DST Block" BADD00000-01717-5705-00001) was reviewed to evaluate potential correlation between preexisting fractures and the observed scaling zones. Results from this review were inconclusive. The identified zones of loose rock exist in locations with representaive surface fractures based on pre-test fracture mapping of the Heated Drift. Thermal, hydrologic, and acoustic emission observations in the local rock mass above the roof of the Heated Drift at about 10 to 12 m from the bulkhead appear to coincide with a distinct set of fractures (Thermal Test (Informal) Progress Report #5, April 9, 2000). This anomalous behavior of fractures appears to be in close proximity to two of the four identified scaling zones. A more definitive assessment of the fractures in the DST block and their association with the scaling zones may provide additional insight about the observed scaling.

Aggressive Heating

To relate the observations in the DST to the potential repository system, conditional differences need to be assessed. The areal thermal loading for the DST is estimated to be at least six times greater than the EDA-II design. This factor of six would nearly double for the alternative low-temperature design for a potential repository. This aggressive heating allows the DST to be conducted in a reasonable amount of time, which would not be the case if the heating rate for the potential repository was used. Ultimately, this aggressive heating allows the DST to drive the thermal-hydrological-mechanical-chemical processes in a readily observable manner so that the Project can refine its understanding of coupled processes and quantitatively test the process models.

Also, it should be noted that correlation between mineral transformations, including cristobalite and tridymite, and the observed scaling does not appear to exist. This assessment is based, in part, in the apparent mechanical stability of the wing heater

boreholes which are surrounded by the highest rock temperatures (approximately 230 °C) in the DST block.

Potential for Stress Failure in the Heated Rock

In the Heated Drift, heating increases horizontal thermal stresses because horizontal constraints are substantial especially when compared to vertical constraints. Constraint in the horizontal direction, although reduced by the presence of discontinuities, are increased in the regions above the Heated Drift by the widespread influence of the two sets of wing heaters on either side of the Heated Drift. The maximum increase in rock temperature along the roof of the Heated Drift is approximately 180 ^{0}C. These wing heaters were designed to thermally constrain the Heated Drift in a manner not unlike that anticipated for potential repository emplacement drifts surrounded by additional heat-generating emplacement drifts. Even when rock mass thermal expansion and modulus are considered, which account for discontinuities/fractures, horizontal stresses become much higher than the vertical stresses during the heating phase of the DST. Evidence of a differential stress state that includes higher horizontal stresses is found in the displacement measurements of the concrete liner in the Heated Drift. The combination of horizontal closure and vertical elongation results in "ovalization" of the Heated Drift. Since the ambient in-situ stress state at Yucca Mountain is nonlithostatic with the maximum principal stress in the vertical direction, a transient reversal of principal stress occurs during heating of the DST. Also, pre-test calculations indicate the circumferential or hoop stress in the roof of the Heated Drift can be 70 Mpa, whereas the vertical stress in the nearby rock will not exceed 7 Mpa. These stress conditions can induce fracturing parallel to the surface of the Heated Drift that result in small slab-shaped fragments of rock akin to those observed in the scaling zones. In summary, rock failure along the roof of the Heated Drift is possible given the maximum change in temperature of 180 ^{0}C, high stresses concentrations that exist along the rough surfaces of the Heated Drift, and the lack of confinement along the drift's periphery.

Multiple Point Borehole Extensometer (MPBX) Data

Three arrays of MPBXs were installed in the Heated Drift roof to measure displacement of the rock due to thermal expansion and the resulting stress changes in the host rock. The displacement measurements are taken by linear variable displacement transducers (LVDTs) located at the collar mounted at the opening of the borehole on the drift wall. The LVDTs are connected by Invar rods to anchors within the borehole. These anchors are located approximately 1, 2, 4, and 15 meters from the collar. One of the MPBX arrays (MPBX-3) is located approximately 13.7 m from the bulkhead, where the two zones of scaling are observed Figure 2. A second array (MPBX-7) is located approximately 21 m from the bulkhead where it appears scaling may exist but is too difficult to assess because of distance and limited illumination. The third array of MPBX boreholes is located in the concrete liner, which remains intact, approximately 41.0 m from the bulkhead.

The MPBX data are expected to show that the rock expands in a manner consistent with thermoelastic behavior, with a steadily increasing displacement between the anchors and the collar. This increase in displacement is produced by the heated rock expanding into the drift, while the cooler rock further away remains relatively unchanged. As the thermal

pulse expands away from the drift, these displacements continue to increase. This pattern is predicted by pre-test thermal-mechanical analyses performed by the thermal test team ("Drift Scale Test Design and Forecast Results", BAB000000-01717-4600-00007). Observed deviations from this elastic pattern might signify "events" that could indicate the creation of a fracture, or sudden slippage along an existing fracture. A sudden decrease or increase in displacement in the MPBX data is a potential marker for such an event. Thus, the MPBX data can be used to determine if the scaling observed in the Heated Drift thus far is significant.

Figures 7 and 8 show the MPBX measurements through March 2001 for MPBX-3 (borehole 147, 13.7 m from the bulkhead) and MPBX-7 (borehole 154, 21.0 m from the bulkhead). Both of these MPBXs are anchored in the roof in boreholes oriented at 30-degree angles from the vertical. These MPBX are both on the right side of the crown centerline if one is looking into the Heated Drift.

The video recorded on May 2, 2001 show that MPBX-3 is near one of the scaling zones. In general, the data from MPBX-3 (see Figure 3) show a steadily increasing displacement between the anchors and the collar. Anchors 1, 2, and 3 exhibit no sudden changes in displacement since October 23, 2000 (heating day: 1054), which was the date of the previous rail camera run. If a rock fall of significant magnitude to dislodge the collar for MPBX-3 had occurred, there would be sudden changes in all four anchors. One event, however, has occurred with MPBX-3 that is probably not related to scaling. Anchor 4 of MPBX-3 (15m from the collar) has a sudden change to its displacement curve beginning on day 1064 (November 3, 2000), beginning a steady descent, but the other 3 anchors below it do not display similar behavior. Therefore, this displacement behavior for anchor 4 appears to be unrelated to the scaling discussed herein, but it may be attributed to slippage.

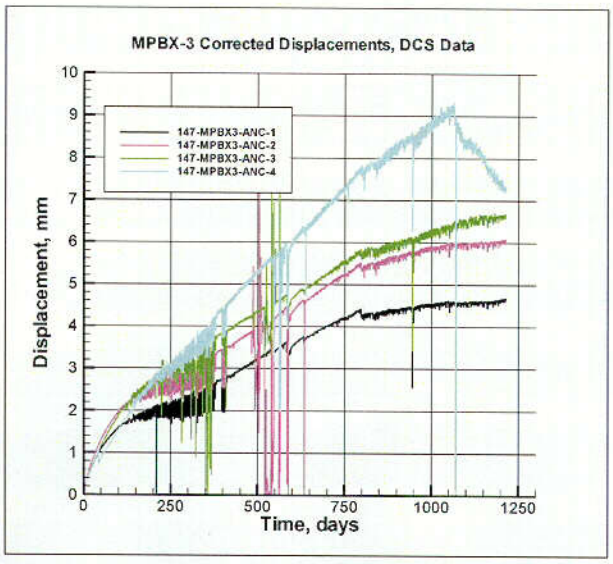

Figure 7. Displacement History of Rock Above the Heated Drift Located Approximately 14 m From the DST Bulkhead (Note: noise in the data is not associated with observed scaling zones).

C08

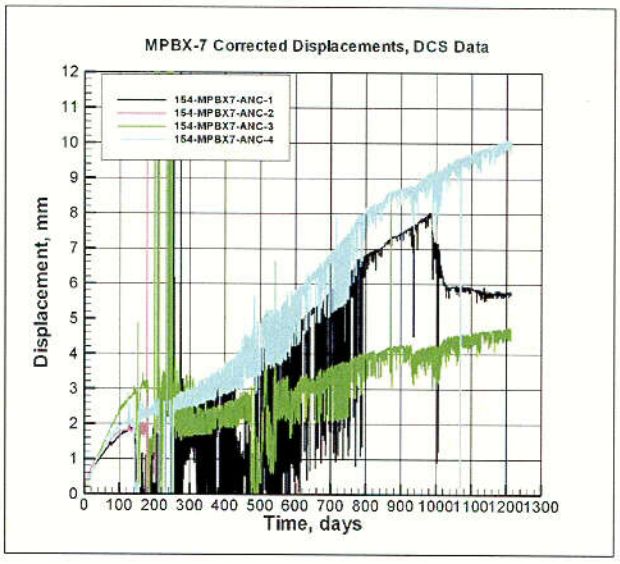

Figure 8. Displacement History of Rock above the DST Heated Drift Located Approximately 21 Meters From the Bulkhead (Note: noise in the data is not associated with observed scaling zones).

One event in the MPBX data that has possible ties to scaling is shown in the data from MPBX-7 (21 m from the bulkhead - see Figure 4). Note that Anchor 1 of MPBX-7 (1m from the collar) begins an abrupt drop in displacement of about 2 mm beginning about day 985 (August 14, 2000). One possible explanation of this drop is a slight loosening of the rock around Anchor 1. However, there is not enough evidence to state this for a certainty. Anchors 3 and 4 do not show a similar sudden change at this time (Note: Anchor 2 failed earlier in the test). This would indicate that the collar was unaffected by any possible rock movement suggesting the volume of rock affected by fracturing is relatively small. Indeed, the other four MPBXs (MPBX-4, MPBX-5, MPBX-8, and MPBX-9) in the roof at these two stations (13.7 m and 21.0 m from the bulkhead) do not display this behavior. Therefore, it can be concluded that the scaling observed to date is probably due to surface effects that involves only a relatively small volume of rock.

Future Activities

- Inspect the Heated Drift weekly with Test Coordination Office personnel and note any changes in scaling along the roof of the Heated Drift.
- Expand observations and analyses of the scaling zones identified in the Heated Drift during the Thermal Test Workshop to be held in Las Vegas on June 7th and 8th, 2001.
- Continue observations and analyses of the scaling in the Heated Drift using available equipment and data such as remote and telephoto cameras, MPBX sensors, and AE measurements.

C09

- Conduct post-mortem examination to assess correlation of scaling along smooth surfaces found in wing heater boreholes and scaling along rough surfaces found in the Heated Drift. This post-mortem examination will also more definitively determine if the rock separation occurred along natural joint surfaces or failed matrix surfaces.
- Consider documentation of scaling observations under ambient/non-heated conditions in excavations throughout the ESF and ECRB including observed rock fragments near the ECRB bulkhead and Tptpmn roof behavior in Alcoves 5, 6, and 7.
- Investigate methods to better illuminate the roof further into the Heated Drift thereby enabling further characterization of scaling.
- Investigate the anomalous thermal, hydrological, and mechanical behavior associated with fractures located 10 to 12 m from the bulkhead to determine if any correlation exists with the observed scaling zones.
- Consider analyses of actual and design loadings of the ground support system in the Heated Drift.

2.2 DST Camera Run 8/16/01

On Thursday morning, 8/16/01, at 0900 hours, a DST remote video camera run was conducted within the Heated Drift. The run was a full scan from within the bulkhead (center of view = 1.3 m) to just about the end of the liner (center of view = 42.5), rotating 340 degrees at each station. This run was conducted using anew lighting system that employed 2 500 watt halogen lights replacing a single 40 watt incandescent bulb. These new halogen lights improved the quality of the video significantly. In attendance were Jim Aamodt, Dan Neubauer, and Gene Griego, all of the Test Coordination Office. No significant differences in loose rock locations or quantity were noted by the team from the run conducted on 5/2/01 other than the two observations noted on 6/12/01 and 6/21/01 (recorded in SN-LANL-SCI-096-V1 under those dates). Videos of the run were distributed to Bob Jones, Steve Sobolik, and Steve Blair.

2.3 Proposed Thermal Test Measurement Report

Scope of Work

The purpose of the Proposed Thermal Test Measurement report planned for FY-02 for the Drift Scale Test (DST), Single Heater Test (SHT), and Large Block Test (LBT) has five distinct tasks:

1. Identify all measurements and, to the extent practicable, graphically display all measurements or representative cross-section of measurements from the DST, SHT, and LBT.
2. Assess uncertainties for each type of thermal test (DST, SHT and LBT) measurement.
3. Determine anomalous and irregular behavior of thermal test measurements and adjust or "smooth" as appropriate
4. Centralize all DTNs of thermal test measurements into a single document.
5. Address the applicability of thermal test measurements toward alternative repository designs including the Lower-Temperature (L-T) design considered in Volume 3 of the SRCR.

The identification of all measurements (thermal-hydrological-chemical-mechanical) from the three thermal tests provides a baseline of information from which the subsequent activities (2 through 5) will be linked. Since the SHT and LBT are completed, the identification of measurements will be complete, whereas for the DST only those measurements from the heating phase will be identified. Because of the numerous sensors, especially in the DST, it may be impracticable to provide graphical displays of all the measurements. Therefore, if the number of measurements becomes too unwieldy, the graphical display will be limited to a representative cross-section.

The evaluation of uncertainty of thermal test measurements is needed because AMRs are focused primarily on numerical simulations in which discussion of uncertainties is limited and rarely address uncertainties of measurements used in model validation. It has been more than three years since any thermal test measurements have been formally documented and discussed (DST Progress Report No. 1). Even then, discussion of uncertainty was not emphasized. Additionally, the DOE has recently recognized the importance of understanding uncertainties that has led to the development of an ongoing uncertainty initiative for the YMP. Furthermore, these measurement uncertainties were also raised by the NRC at recent TEF/ENFE KTI meeting.

A by-product of the evaluation of uncertainties will be identification of anomalous or irregular responses. In the more blatant cases, the measurements will be adjusted or "smoothed" such that these measurements can be used in comparative evaluations with corresponding numerical simulations. For example, some of the MPBX measurements from the DST are irregular because of temperature fluctuations in the mechanical

boreholes. An examination of this data resulted in adjustments which are both beneficial and defendable. Although this exercise of identifying and adjusting measurements has been started, discussed in thermal test workshops, and documented in informal progress reports; documentation in a formal, qualified report does not currently exist. During this activity, irregular behavior that reflects heterogeneity of the test block will also be identified and discussed.

A need also exists to centralize all DTNs associated with the thermal tests. Currently, fractions of all DTNs are cited in numerous documents resulting in cumbersome retrieval of one or several DTNs. This centralization will provide complete histories of thermal, mechanical, hydrological, and chemical measurements from the SHT, DST, and LBT. This activity will include laboratory and field measurements from pre-test characterization as well as integrated (data collection system) and non-integrated measurements, as appropriate, from pre-test, heating, cooling, and posttest periods. When completed, this centralization of DTNs from thermal test measurements will facilitate access of the thermal test measurements by the thermal test team, end-users, and other interested entities such as the NRC and NWTRB.

The final activity involves addressing the applicability of thermal test measurements toward alternative repository designs including the cooler design currently under consideration in the flexible design approach. The thermal tests (SHT, DST, LBT) were designed to ensure the range of responses associated with the four processes (T-H-M-C) considered would be applicable to any repository design including EDA II and the Lower-Temperature (L-T) designs. This attribute of the thermal tests is consistent with the primary objective "to develop a more in-depth understanding of the coupled processes (T-H-M-C) anticipated to exist in the rock mass surrounding the potential repository". Consequently, the applicability of the thermal tests is anticipated to be valid despite changes in repository design such as lower thermal loading and configuration alterations The aspect of the L-T design not directly addressed in the thermal tests is forced ventilation. Therefore, this activity will provide a detailed explanation of the thermal tests applicability to the L-T design in terms of T-H-M-C measurements that are available to validate the TH, THM, and THC models currently under development. This discussion will include the heating/cooling periods of the thermal tests as well as the pre-test characterization of the respective test blocks from laboratory and field measurements. Also, the impact of forced ventilation on these data will be addressed. For example, forced ventilation will reduce temperatures, alter thermal gradients, remove moisture, and slowdown chemical reactions, but may not significantly change the applicability of the thermal tests in validating models of coupled processes. In summary, this activity will address the applicability of T-H-M-C measurements to the L-T design, while related AMRs (TH, THC, and THC) will address ramifications of the L-T design to process models.

Breakdown of Activities for Preparation of the Document

1. Initiate activity including prepare/review/complete the planning document and Technical Change Request
2. Conduct Task 1
3. Conduct Task 2
4. Conduct Task 3
5. Conduct Task 4
6. Conduct Task 5
7. Prepare document under AP-3.11Q. including internal reviews
8. Conduct checking
9. Conduct 2.14 reviews
10. Complete document including Engineering Document and Document Control processing

3. Thermal Processes

Five sections comprise this chapter on Thermal Processes. The topics discussed are thermal data, a white paper that describes DOE's position regarding heat and mass flow through the bulkhead in the Drift Scale Test, a summary of results from the humidity and temperature data acquired July 18th and 19th outside the bulkhead, predictions for the cooling process, and the cooling schedule.

3.1 Thermal Data from the Drift Scale Test Through May 31, 2001

Figure 9 illustrates the sum of all the canister and wing heater power levels during the test. For the first 820 days of the test, the power was reasonably constant dropping from and initial value of about 188 kW to about 178 kW. On 3/2/2000 the first of four intentional power reductions was implemented. The fourth reduction in power was implemented on 5/1/2001. After all four reductions, the total power was approximately 144 kW, or approximately 77% of its initial level. These power reductions were imposed in order to maintain the nominal temperature of the drift wall at a constant temperature of approximately 200 °C.

Figures 10 and 11 illustrate the temperatures recorded on the periphery of the heated drift as a function of time. Ignoring brief, unintentional interruptions to heater power, the driftwall temperature rose steadily until the intentional power reductions were implemented. Since then, these temperatures have remained nearly constant with the driftwall temperature ranging from a low of 189 to a high 208 °C.

Figure 12 illustrates the temperature distribution on the walls of the heated drift on day 1243, the last day for which data were available. Temperatures are coolest near the bulkhead and at the far end of the drift, and warmest on the ribs half way down the drift. The ribs tend to be warmer because of their proximity to the wing heaters. The reference temperature sensor, located in the crown of the drift 25 meters from the bulkhead is at 201.4°C.

Figure 13 illustrates the temperature as a function of distance along the Y – coordinate direction in borehole 79. This borehole is oriented parallel to the Y-coordinate direction at approximately X = 9.5 meters and Z = 3 meters. It runs the length of the heated drift and is located roughly 3 meters above the inner and outer elements of the wing heaters in the right rib of the drift. In Figure 13, the lowest-most curve illustrates the temperatures recorded in the borehole just prior to heater activation and subsequent curves portray the temperatures every 30 days thereafter. During the first few months, the curves have an upward curvature which reflects the fact that this borehole is slightly downwardly inclined which places the deeper parts of the borehole somewhat closer to the wing heaters. Most of the curves also show an oscillatory behavior with every other temperature measurement being slightly warmer than the intervening measurements.

There are two other thermal behaviors evident in Figure 13. The first is the tendency of the curves to flatten significantly at 96 °C, the boiling point of water at this elevation.

This occurs because the temperature readings tend to pause temporally at the boiling point as the water in the rock evaporates nearly isothermally.

The second interesting thermal signature evident in Figure 13 is the temperature behavior near Y = 11 meters. At sub-boiling temperatures the rock near this location was substantially warmer than the rock on either side of it. Near the boiling point, the temperature profile was essentially constant, and at temperatures exceeding the boiling point the rock near this location was somewhat cooler than the surrounding rock. A possible explanation for this behavior is the existence of a vertical fracture near this location. When the rock temperature was below boiling (i.e. the rock still contained liquid water), steam generated below this location (closer to the heater), may have been rising along the fracture, elevating the temperature of the rock near the fracture to levels exceeding those of adjacent rocks. At boiling, everything was isothermal for awhile as water in the rock evaporated. After all the water in the rock had boiled off, the temperature of most of the rock started to increase again. Near the fracture however, the temperature remained somewhat cooler than that of the surrounding rock. It may be that a lot of water condensed in this region when the temperature was sub-boiling and additional heat was required to evaporate that water when the temperature in the vicinity of the fracture first reached and then exceeded the boiling temperature. Alternatively, the anomalously cool temperature near the fracture could reflect cool material flowing downward in the fracture toward the heated region.

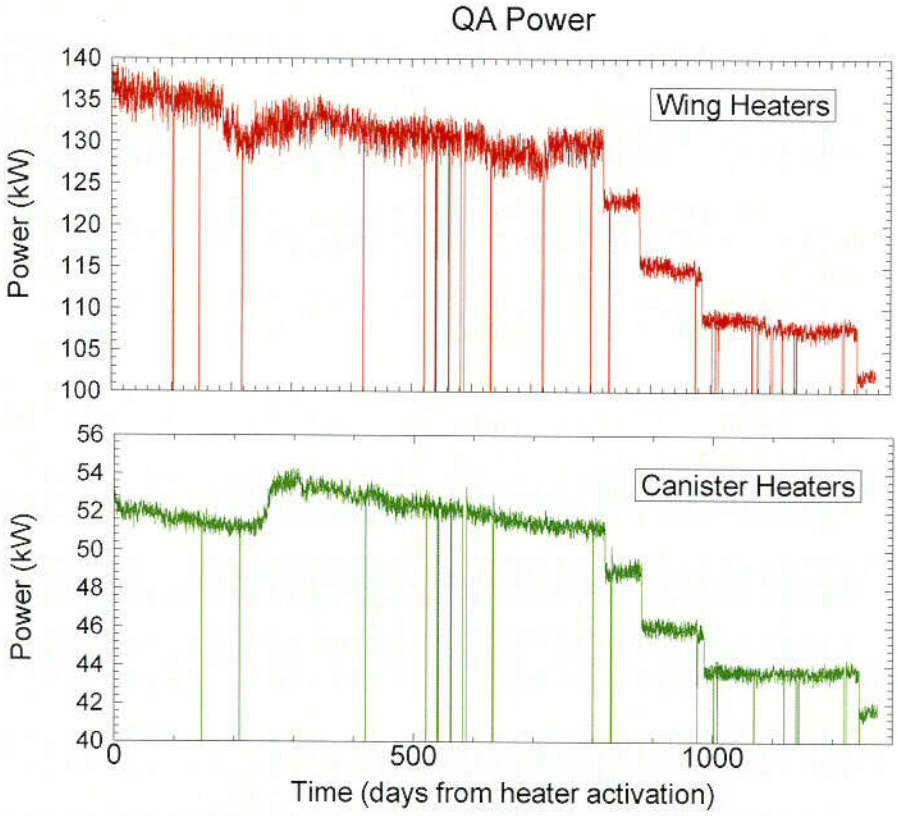

Figure 9. Measured Wing Heater and Canister Power

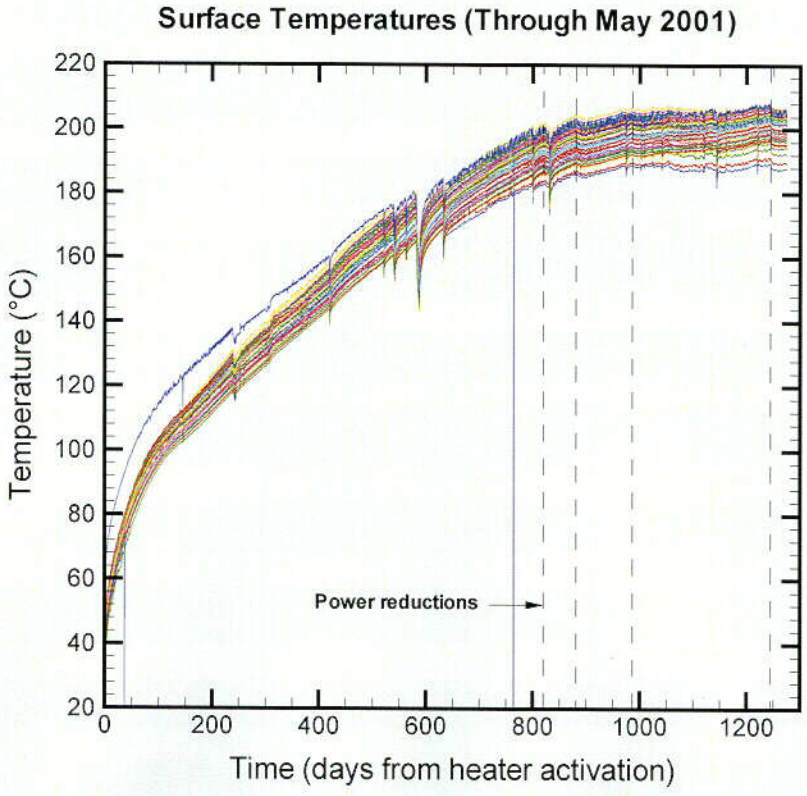

Figure 10. Measured Temperatures Along Periphery of Heated Drift

C10

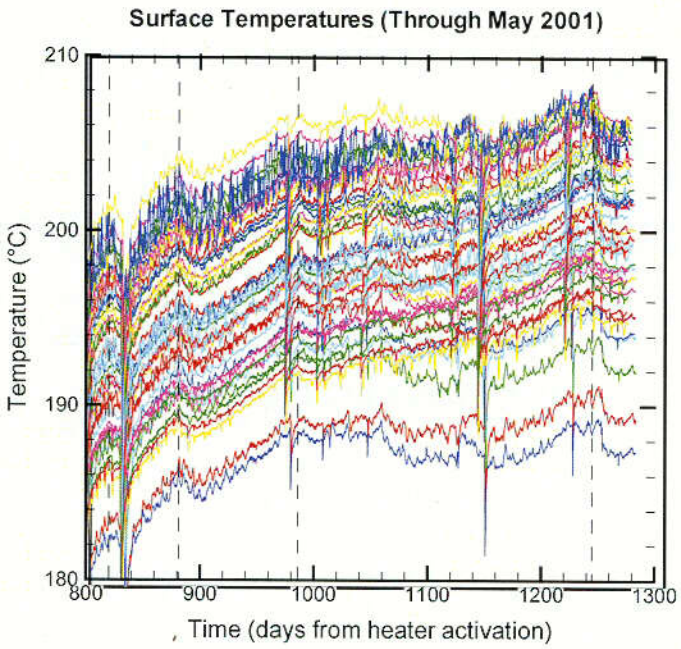

Figure 11. Measured Temperatures Along Periphery of Heated Drift - Details

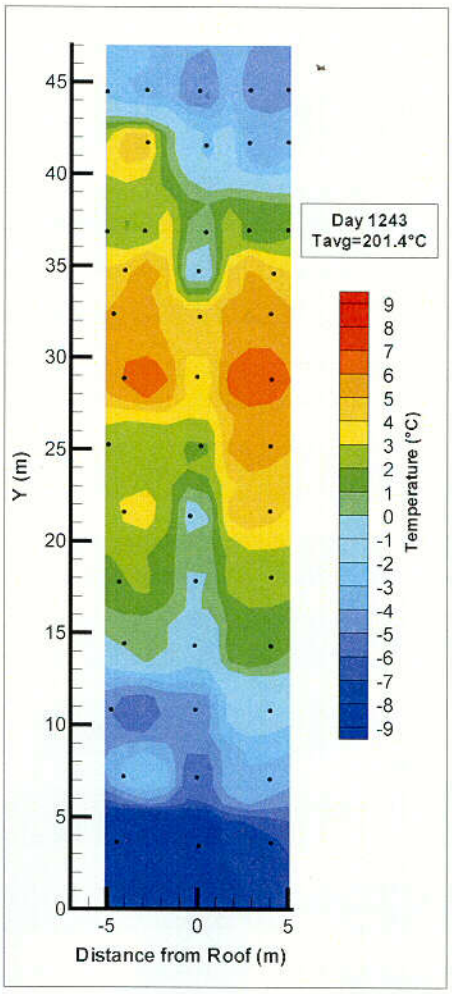

Figure 12. Measured Temperature Distribution Along Periphery of Heated Drift

C11

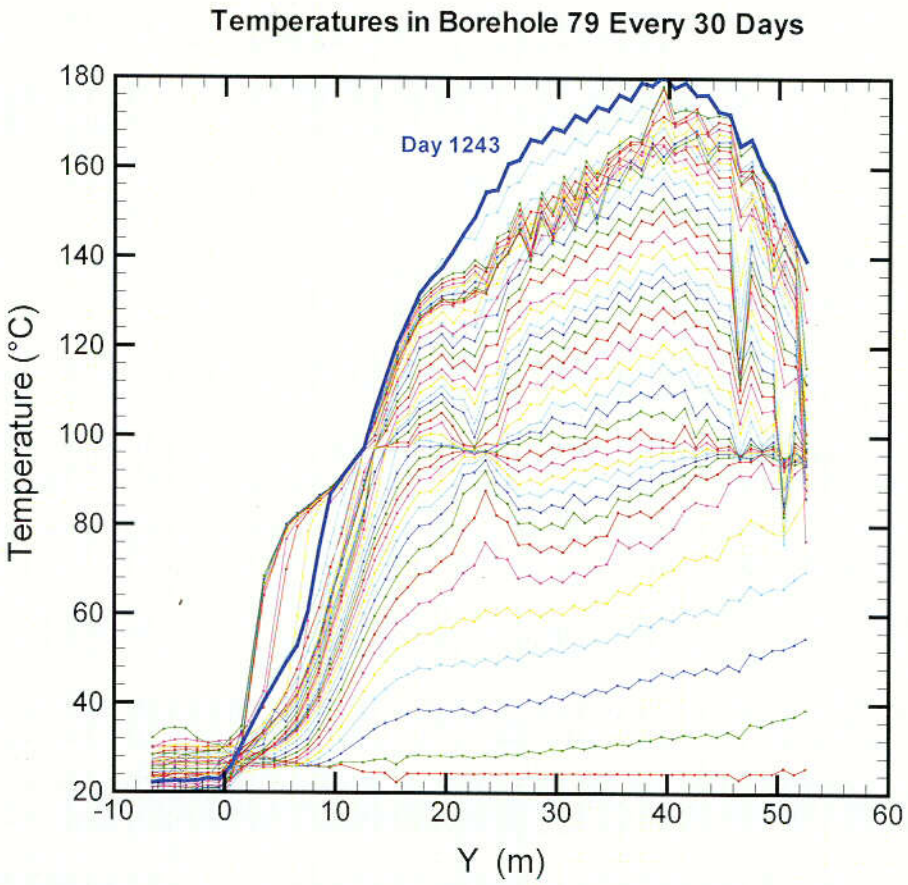

Figure 13. Measured Temperatures in Borehole 79 at 30 Day Intervals

C12

3.2 Heat and Mass Flow Through the Bulkhead in the Drift Scale Test

3.2.1 Introduction

This white paper satisfies the agreement (TEF 2.1) reached between DOE and the NRC at the January 2001 Technical Exchange on Thermal Effects on Flow. The assessment of heat and mass loss through the bulkhead of the Drift Scale Test (DST) has been ongoing for approximately five years, has been well documented (see Section 3.2.3), and has been discussed openly, including at thermal test workshops. Because of this continuous and open interchange, the discussion in this white paper assumes that the reader is thoroughly familiar with the subject matter, and is presented in an informal style. By delineating DOE's position in a white paper rather than a formal technical report, the technical discussion is focussed on the specific information and assessments relevant to the key technical issue being addressed.

The main objective of the DST is to acquire a more in-depth understanding of the thermally driven coupled processes in the potential repository rocks. To meet this objective the DOE takes an approach of a close integration between modeling and measurements. Thermal-hydrological (TH) numerical models were constructed for the DST and test results were predicted prior to the commencement of the test. As the test progresses, test data are continuously being evaluated and compared to the model predictions. The level of agreement between the modeled and measured data of temperature and liquid saturation in the test block is used as a direct test of the models developed and provides basic insight into the thermal-hydrological processes.

The bulkhead separating the hot side of the Heated Drift from the unheated section is not perfectly sealed because bundles of power cable and instrument-wiring pass through the bulkhead (CRWMS M&O 1998a). The unsealed bulkhead acting as an open boundary for unmonitored heat and mass flow introduces an artifact in the test. The DOE's position is that the coupled processes are understood well enough to analyze this artifact quantitatively. The first three years of data support the validation of DST thermal-hydrological coupled-process models and current treatment of mass and energy loss through the bulkhead. Based on an assessment of the impact of the unmonitored heat/mass flow through the bulkhead on the DST results, the DOE's position is that these impacts are small enough that a measurement of heat and mass losses through the bulkhead of the DST does not appear necessary.

The DST results are intended for validation of models of thermally driven coupled processes in the rock, and measurements are not directly incorporated into TSPA models. In this white paper, the technical bases are delineated for the DOE's understanding of heat and mass losses through the bulkhead, the effects of these losses on the test results, and the decision regarding measurements of heat and mass losses through the DST bulkhead. In addition, this paper also addresses uncertainty in the fate of thermally mobilized water in the DST and the effect of this uncertainty on conclusions drawn from the DST results.

3.2.2 Summary and Conclusions

Summary highlights of this white paper include the following:

1. Background information on the issue of heat and mass loss through the DST bulkhead is provided including (1) its identification, (2) steps taken by the DOE to address it, and (3) prior interactions between the DOE and the NRC on this issue.
2. Summation of completed measurements and a determination that complete and accurate measurement of heat and mass flow through the bulkhead is intrinsically difficult, uncertain, and unnecessary.
3. The DOE uses close integration between modeling and measurements in the DST to gain a more in-depth understanding of the thermal and hydrological processes in the repository rocks. Pre-test simulations were carried out to predict the outcome of the DST. DST data are being utilized to iteratively evaluate the accuracy of numerical models.
4. The DST TH models include:
    a. Open-boundary conditions throughout the DST modeled region.
    b. Radiative heat transfer from the canister heaters to the walls of the Heated Drift that is assumed to be 100 percent effective.
    c. Treatment of the rock matrix and fractures as two separate interacting continua.

    Prior to incorporating explicitly the wing-heater boreholes, a positive mean error for the DST thermal comparative analyses (of less than 15%) indicated that not all heat losses, including those through the bulkhead, were considered in the conceptual model.
5. The revised model treats the Heated Drift and the wing-heater boreholes as high-permeability conduits, allowing part of the vapor generated in the rock to pass through the bulkhead. Sensitivity studies show that for this different conceptual implementation of the open-boundary bulkhead, the mean error of the simulated and measured temperatures for approximately 1,700 sensors is reasonably small (a few $^{\circ}C$ after 30 months of heating), indicating that the open-boundary representation for the bulkhead is appropriate.
6. The present understanding, based on global energy balance considerations applied to both simulated results and measured quantities within the rock mass, is that more than 70 percent of total heat input serves to raise the temperature of the rock, with the remainder shared between raising the temperature of water to boiling and vaporizing the water.
7. The model results also show that of all the vapor produced from heating, about a third moves to cooler regions of the rock mass and condenses, while the rest is lost through the bulkhead via the Heated Drift. If the DST were a totally closed system, then the zones of increased liquid saturation in the test block would contain possibly three times the volume of water.
8. Locations of dry-out and condensation deduced from ERT, GPR, neutron logs and air permeability in general corroborate well with the simulated time evolution of the liquid-saturation changes in the matrix and fractures. This

indicates that the modeling has captured the fate of the thermally mobilized water for the open-system DST despite the measurement uncertainty of the bulkhead heat loss.

9. Uncertainty in the fate of thermally mobilized water is discussed both implicitly and explicitly throughout this white paper. In summary, the uncertainty associated with the understanding of moisture redistribution in the DST is considered to be acceptable based on good agreement in the thermal and hydrological comparative analyses of corresponding measurements and simulations and other observations discussed in this white paper.
10. The favorable comparison of the DST models and observations for both temperatures and bulk moisture redistribution demonstrates that all the major components of the thermal hydrological processes are included in the TH process models (including the leakage through the bulkhead). Therefore the objectives of acquiring a more in-depth understanding of the coupled processes and validating the conceptual thermohydrological processes at a drift scale are being met in the DST.

In conclusion, the DST is large-scale, open-system, field test in which many intrinsic uncertainties exist including those associated with material properties, fracture characteristics, conceptualization in the process models, initial conditions as well as the boundary condition along the bulkhead. Despite these uncertainties, it is possible to satisfy the primary objective of the DST, which is to obtain a more in-depth understanding of coupled thermal-hydrological-mechanical-chemical processes anticipated to exist in the local rock mass surrounding the potential repository at Yucca Mountain. Specifically, this white paper has identified several advances in the understanding of coupled TH processes (as per the above summary and detailed discussion in Sections 3 through 5) despite the uncertainty of the boundary condition along the DST bulkhead. Consequently, the DST continues to serves as a key validation tool of relevant process models, including the TH models, even though intrinsic uncertainties exist such as those associated with the heat and mass loss through the bulkhead.

3.2.3 Background

The issue of heat and mass loss through the DST bulkhead has been ongoing since the design of the DST approximately 5 years ago, a design in which the primary purpose of the bulkhead was to act as a thermal barrier (CRWMS M&O 1996) that includes safety considerations. Pre-test numerical simulations of the DST resulted in concerns about unmonitored heat and mass loss through the thermal bulkhead (Buscheck and Nitao, 1995). Recommendations included isolating the DST Heated Drift from direct pneumatic interference with the ESF tunnel system. This precaution was in itself problematic since safety concerns would develop if the pressure within the DST heated drift were allowed to increase.

On December 3, 1997, the heating of the DST was initiated. Within 40 days of the start of heating, moisture started to flow out of the bulkhead, as evidenced by condensation on

various surfaces on the cool side of the bulkhead. This behavior was consistent with the heating of a large volume of rock that is highly fractured and approximately 90 percent saturated. As water in the rock boiled and turned to steam, the vapor moved under pressure gradient into cooler rocks, as well as into the Heated Drift and through the bulkhead. Also, the observed wetting on the cool side of the bulkhead alternated with drier conditions, with the latter coinciding with low relative humidity readings in the Heated Drift. Upon investigation, it became evident that barometric pumping was the cause for the intermittent wetting (Datta, 1998). Gas phase flow from the rock to the Heated Drift is driven by pressure gradient. Superimpose on the positive pressure gradient from the rock to the Heated Drift is the barometric pressure fluctuations. Therefore, as barometric pressure decreased, more vapor flowed from the rock into the Heated Drift and out the permeable bulkhead, while also increasing the relative humidity in the Heated Drift. Conversely, as the barometric pressure increased, less vapor flowed from the rock into the Heated Drift and the relative humidity decreased. Indeed, the relative humidity measurements in the Heated Drift vary inversely as the barometric pressure.

As the DST progressed into its second year of heating, the DOE decided to focus on heat and mass loss through the bulkhead and two other technical issues in a DOE/NRC Appendix 7 meeting held in Las Vegas on April 28, 1999 (CRWMS M&O 1999a). Many of the details of NRC's concerns presented at the meeting were documented later in the year in Revision 2 of the Issue Resolution Status Report (IRSR) on the Key Technical Issue (KTI) for Thermal Effects on Flow (NRC 1999). Discussion at the Appendix 7 meeting included approaches used to measure both the conductive and convective heat losses through the bulkhead. NRC concurred with the proposed remedies to address conductive heat loss. These remedies consisted of either installing permanent heat flux meters to the bulkhead or insulating the cool side of the bulkhead.

Agreement was also reached regarding remedies to address convective heat loss. These remedies included sealing the bulkhead and proposed modifications of the existing system to measure convective heat loss. Modifications included continuous monitoring of water vapor flow through one or two small openings in the bulkhead. Also, it was agreed that the moisture monitoring data collected by LBNL for the Ambient Moisture Monitoring Program of the Exploratory Studies Facility would be evaluated to estimate moisture losses. Specifically, the plan was to utilize the relative humidity data in the cool side of the bulkhead from the Moisture Monitoring Program to estimate the moisture loss from the DST. However, the thermal test team concluded that the operational ventilation flow rates (between 50 and 150 million liters per hour) imposed just outside of the Heated Drift are too large to allow a direct measurement of changes in the monitored humidity data (Wagner 1999).

Between July 1998 and May 1999, several measurements of conductive and convective heat loss through the bulkhead were conducted (CRWMS M&O 1998b, 1999b, 1999c). Although these measurements were intended to quantify the losses, they also provided much insight into the difficulty of obtaining complete and precise measurements of conductive and convective losses. In October 1999, an Interoffice Correspondence (IOC)

was prepared that summarized the findings to date (Wagner 1999). In summary, the original plan/design of the DST bulkhead was still considered satisfactory. The bulkhead was simply intended to provide a protective and primary thermal barrier to allow personnel, both visitors and workers, to observe the Heated Drift and to work in close proximity to the bulkhead/Heated Drift with minimal risk. After much scrutiny including determination of the difficulty in sealing the bulkhead, measurement of conductive and convective heat losses, simulation of the DST, and analyses of the measured and simulated behavior, it was determined that extensive and more accurate characterization of the heat loss through the bulkhead would be unnecessary as well as difficult and problematic. The October 1999 IOC concluded that the need to measure heat loss through the bulkhead depended on the accuracy of numerically simulating the thermal behavior in the DST. Analyses up to that time indicated that an assumed convective boundary condition resulted in good (within 15 percent) comparative agreement between measured and simulated temperatures. Thus, the artifact of heat and mass loss through this permeable boundary appeared to be properly modeled.

In March 2000, the DOE released a letter to the NRC that addressed Revision 2 of the IRSR on the KTI for Thermal Effects on Flow (DOE 2000). Included in this letter was discussion on heat and mass loss through the DST bulkhead. Basically, the discussion cited in the prior IOC (Wagner 1999) was reiterated, along with additional statements regarding the NRC document.

In the past five months, additional sensitivity calculations have been conducted to investigate the effect of convective losses from the wing-heater boreholes and the effect of barometric pumping (CRWMS M&O 2001a). These calculations have furthered the thermal test team's understanding of heat-and-mass loss effects through the bulkhead. Revision 3 of the IRSR for KTIs on the TEF, which is the most current IRSR, reflects much of the more recent discussions cited above (NRC 2000). Also, related discussions at the Technical Exchange (held in Pleasanton, CA January 8-9, 2001) have been documented (CRWMS M&O 2001b). It was noted at this meeting that heat (energy) and mass losses need to be addressed in future thermal tests such as the Cross-Drift Thermal Test. This test, although not scheduled, may begin within the next 18 months.

3.2.4. Measuring the Heat and Mass Flow through the Bulkhead

A summary listing of field efforts to address the issue of mass and heat loss through the bulkhead is provided below:

(1) Determination of conductive heat flux by applying a heat flux meter to seven locations on the bulkhead (five measurement locations were steel and two were glass);
(2) Added insulation on the cool side of the bulkhead;
(3) Estimation of convective heat loss by considering how much water vapor was removed from a small diameter pipe in the bulkhead during a 60-minute sampling period;
(4) Sealing of vapor leaks in the bulkhead, such as those in the camera door and cable outlets, to the extent practical.

A letter to the NRC from the DOE (DOE 2000) contained a discussion about the intrinsic difficulty in accurately and precisely measuring a highly heterogeneous moisture and heat flux from a diffuse source loss (DOE 2000). Considerable uncertainty was involved in item (3) above, because it is not known what fraction of moisture loss is captured in the measurement system as a result of the inherent leakage through bundles of power cable and instrument-wiring pathways. An alternate approach (to circumvent this uncertainty) would be to measure the moisture increase in the drift on the cool side of the bulkhead as an estimate of the mass loss from the convective heat flow from the DST. This measurement is nontrivial because of the substantial ventilation on the cool side of the bulkhead and the limitations of relative humidity measuring devices. These initial attempts to directly and to accurately measure the heat and mass loss through the DST bulkhead resulted in a consensus among the thermal test team that it was a difficult task. More importantly, based largely on the following discussion, a direct measurement of the heat and mass loss through the bulkhead is not needed to satisfy the primary objective of the DST.

3.2.5 Thermal-Hydrological Modeling of the Drift Scale Test

3.2.5.1. Design and Pre-Test Simulations

As was mentioned previously, the objective of the DST is to acquire a more in-depth understanding of the thermally driven coupled processes. The approach is to implement a close integration between modeling and measurements. Modeling was involved in both the design and pre-heating phases of the DST, and continues throughout the test (CRWMS M&O 1998). Scoping calculations guided the design of the DST, particularly in determining the location of instrumented boreholes for monitoring the thermal, hydrological, mechanical, and chemical responses. Pre-test simulations to predict the outcome of the planned 8-year test accounted for realistic representation of the complex test geometry (as designed) in three-dimensions, using rock properties that were calibrated to site-specific pre-test characterization measurements. For modeling of the thermal hydrological processes (coupled transport of water, water vapor, air, and heat in heterogeneous porous and fractured media) the numerical tools used are the simulators TOUGH2 and NUFT. Both numerical codes account for the movement of gaseous and liquid phases (under pressure, viscosity, and gravity forces), transport of latent and sensible heat, and phase transition between liquid and vapor. Strict mass and energy balance is adhered to for every gridblock.

3.2.5.2 Interim Status of the DST Thermal-Hydrological (TH) Model

DST data are being utilized to iteratively re-evaluate the accuracy of the numerical model. Modifications since the pre-test conceptual/numerical model for the DST include representation of test configuration (such as as-built borehole and sensor locations) and test conditions (such as power input) that were not available when pre-test simulations were performed. Also, for certain elements in the conceptual model, it was possible to discriminate between alternative assumptions that were studied in the pre-heat predictions

based on the first few months of heating-phase data. Hence, in the model, the assumptions and hypotheses supported by the measured data have been adopted. The continuous refinement of the conceptual/numerical model, based on a close integration of modeled prediction and measured data, led to the following model definition :

(1) **Open-boundary conditions exist throughout the DST modeled region.** These boundary conditions allow heat and moisture to flow through the boundaries to the Observation Drift, and through the bulkhead connecting the hot side of the Heated Drift to the cool side of the Heated Drift. In the pre-test simulations of the DST, a slightly thermally insulated open boundary was implemented on the Observation Drift to allow free flow of fluid; however, the Heated Drift and the thermally insulated bulkhead were treated as closed boundaries; that is, they were assumed to have zero thermal conductivity and be impermeable to fluid flow. A study of the simulated temperature for the first three months of heating indicated that in the immediate vicinity of the Heated Drift a prominent heat pipe should develop, but this was not observed in the measured data. That is, while the pre-test simulations indicated a distinct two-phase zone of water and vapor in the rock mass immediately around the Heated Drift, the measured temperature did not show this isothermal zone. This led the investigators to conclude that the Heated Drift did not act like a closed boundary, but rather as a conduit for vapor to escape. The numerical model was modified to implement the Heated Drift as a high-permeability conduit, and the bulkhead as an open boundary, and as expected, the modeled heat-pipe signature previously generated using the closed boundary disappeared from the simulations. The model shows vapor escaping through the bulkhead via the Heated Drift.

(2) **Radiative heat transfer from the canister heaters to the walls of the Heated Drift is assumed to be 100 percent effective.** Sensitivity studies in the pre-test predictive modeling indicate that the more effective the radiative heat transfer, the more uniform is the temperature distribution along the periphery of the Heated Drift. The first six months of temperature data along the Heated Drift show nearly uniform temperatures around and along the Heated Drift which demonstrates that radiative heat transfer is nearly 100 percent effective.

(3) **The DST thermal hydrological model treats the rock matrix and fractures as two separate interacting continua.** Observations from the Single Heater Test indicated the effective continuum model (ECM) was not suitable because moisture redistribution is better characterized by a TH model that allows the rock matrix and fractures to act as two separate interacting continua. If liquid flow is uniformly distributed in all connected fractures, the entire fracture area is available for coupling of flow between the matrix and fracture, implying rather large fracture-matrix interactions. On the other hand, if only a fraction of the connected fractures actively conduct water, then the interaction between the fractures and matrix is far more limited. Both conceptual models: the former (the conventional dual-permeability model) and the latter (the dual-permeability model with the active fracture option) have been applied to the DST. The two conceptual models produce different flow phenomena. The Active Fracture Model tends to give more gravity drainage of condensate in the fractures and less imbibition into the matrix than the conventional dual-permeability model. This results in a more symmetrical

condensation zone with respect to the heater horizon at early phases of heating than that predicted by the conventional dual permeability model. As the heating phase progresses, both models give rise to a more elongated zone of increased moisture below the heater horizon than above. The differences of the moisture redistribution predicted by these two conceptual models are too subtle to be discriminated by the geophysical data (from electrical resistivity tomography and crosshole radar tomography) for the DST.

A positive mean error for the DST thermal comparative analyses indicated that not all heat losses, including those through the bulkhead, were considered in the conceptual model. This observation was from comparison of simulated and measured temperatures involving approximately 1,700 thermal sensors located throughout the DST block during the first 18 months of heating. The mean error at 6, 12, and 18 months of heating was 0.7, 2.4, and 4.2 °C respectively. Based on the positive mean error for the times and locations considered, it can be argued that the numerical model was not accounting for all the heat losses and predicting too much heat retention in the test block.

3.2.5.3 Heat Losses from the Test Block Based on Model Results

Model results show that a fraction of the vapor generated in the rock mass from heating enters the Heated Drift under a gas pressure gradient and then leaves through the permeable bulkhead. The numerical model explicitly calculates the heat and mass fluxes through every grid-block. Simulations show that the composition of the gas flux crossing the bulkhead boundary is composed almost entirely of vapor, and the heat flux is simply the enthalpy of the gas flux. That is, except for a multiplication constant, the mass and heat flux crossing the bulkhead boundary is one and the same. The vapor leaving the bulkhead carries with it the latent heat of condensation, constituting the dominant source of heat loss from the test. The loss from sensible heat is small compared to the convective heat loss (the difference of modeled conductive heat loss by assuming a perfectly thermally insulating bulkhead and a slightly conductive bulkhead using the thermal conductivity of the insulating fiberglass is about 1kW).

Results from the fourth comparison discussed in section 5.2 are based on a numerical model in which the wing-heater boreholes were modeled as rock with thermal sources inside. Because the Heated Drift acts as a high-permeability conduit for permitting vapor to leave through the bulkhead, it was postulated that the wing heaters could be modeled similarly as high-permeability conduits. Such an approach would allow transfer of additional vapor (and the heat) out through the bulkhead. This behavior was expected to further reduce the modeled temperature in the rock mass.

To test this hypothesis, investigators constructed an alternative DST TH numerical model to include the wing heater numerical gridblocks as high-permeability conduits. Again, the mean error between the simulated and measured temperature field from approximately 1,700 sensors was computed at different phases of heating. For this conceptual model, the values for mean error are 0.01, -0.15, 0.90, 1.06, 1.27 °C respectively at 6, 12, 18, 24, and 30 months of heating. These values are considerably smaller than those in the fourth

comparison discussed in the previous section, where the numerical model did not treat the wing-heater boreholes as preferential high-permeability flow paths. Since the wing-heater boreholes are connected to the Heated Drift, they allow for vapor generated in the rock mass around them to escape to the Heated Drift and subsequently out of the bulkhead. The thermal test team's understanding of the causes of the heat and mass losses through the bulkhead led to this improved conceptual model for the wing-heater boreholes. Given the close agreement of the observed data and the model results, it appears that this approach accounts well for the transfer of the vapor between the rock mass and the open-air conduits to the bulkhead.

Simulations from this conceptual model that treats the wing heater numerical gridblocks as high permeability flow paths predict that the heat flux through the bulkhead peaks between 9 to 12 months of heating at about 38 kW, then steadily declines to around 26 kW at 4 years, the end of the planned heating phase. These numbers should be an upper bound because the model for the DST that treated the 50 wing heaters as a smeared heat source does not model each borehole explicitly. A lower bound would be that of the model in the fourth comparison discussed in the previous section. There the wing-heater boreholes were represented with rock properties, and the heat-loss peaks at about 25 kW and declines to about 16 kW at the end of 4 years of heating (CRWMS M&O 2001a). Precise values of heat loss would also depend on whether the numerical model implements the vapor-pressure lowering effect or not. With the relatively high residual liquid saturation (18%) assumed for the matrix, incorporation of vapor pressure lowering would decrease the volume of vapor generated, and in turn the vapor flow out of the bulkhead. Furthermore, the heat-loss numbers quoted above are for a conceptual model that has not taken into account the barometric pressure fluctuation. Barometric pumping is expected to induce additional vapor loss through the bulkhead. Sensitivity studies by numerical simulations show that barometric pumping may increase the convective heat loss up to 28 percent compared to that from a model with time-independent pressure-boundary conditions (CRWMS M&O 2001a).

Modeled results also show that very little moisture/heat is lost through the open boundary of the Observation Drift. This is the case because of (a) its distance from the heat source (the Observation Drift is parallel to the Heated Drift, its wall 30 m from the center of the Heated Drift and about 15 meters from the end of the wing-heater boreholes), and (b) the absence of high-permeability conduits connecting it to the heat sources. Because of this observation, the Cross-Drift Thermal Test was designed to ensure rock boundaries were a sufficient distance from the heaters (CRWMS M&O 2000).

In most models for the DST, the bulkhead is modeled as perfectly insulated. A sensitivity study assigning non-zero thermal conductivity to the bulkhead shows that the conductive heat loss through the bulkhead is insignificant compared to the convective heat loss. In other words, modeled results show that vapor loss through the bulkhead from the permeable Heated Drift constitutes the majority of the heat loss. Discussion above show that different conceptual variations of the open-boundary bulkhead do not give rise to identical simulated convective heat loss. Alternative conceptual models investigated include closed wing-heater boreholes, implementation of the open wing-heater boreholes

with different approximations, incorporating or ignoring vapor pressure lowering, and effects of barometric pumping. Sensitivity studies show that for the different conceptualizations and combination thereof, the mean error of the simulated and measured temperatures for approximately 1,700 sensors is reasonably small (a few ^{o}C up to 30 months of heating), indicating that the open-boundary assumption for the bulkhead is appropriate.

3.2.5.4 Global Energy Balance

To gain further insight into how the heat input from the canister heaters in the Heated Drift and the wing heaters is partitioned in the rock mass and the pore water, the thermal test team (CRWMS M&O 2001a) applied a global energy accounting to both the numerical model output and the interpolated measured temperature. Energy supplied to the DST is spent in:

(1) raising the temperature of the rock mass,
(2) raising the temperature of the water, and
(3) supplying the heat of water vaporization.

Other energy uses, including heating of the air, are considered negligible. The heat of vaporization is returned to the rock for any water that condenses within the rock mass.

Global accounting is first applied to the numerical model. The numerical model calculates the temperature and liquid saturation for every gridblock at every time step. Consequently, the change in temperature (ΔT) and the change in liquid saturation (ΔS_l) from the start of heating is known for every gridblock at any specified time. Given the porosity, initial liquid saturation, and the initial temperature of the test block; ΔT and the heat capacity of rock and water are needed to compute the contribution to (1) and (2), while ΔS_l and the heat of vaporization are needed to compute the contribution to (3). The global accounting is obtained when contributions to (1), (2) and (3) are summed over all gridbocks. Applying this accounting to numerical model output at two years of heating results in the following energy distribution: 76% for heating up the rock, 12% for heating water, and 12% for vaporizing water.

Global accounting is also applied to the measured temperature. Because the temperature data are too diffusely distributed to interpolate throughout the entire three-dimensional domain, the interpolation has been reduced to a two-dimensional plane and scaled by the length of the Heated Drift. Further, since there was no measurement of S_l for each interpolation gridblock, an assumption was made for assigning ΔS_l according to the temperature measurement for computing (3). The assumption was that whenever temperature was above boiling, the liquid saturation in that interpolation gridblock was given a residual liquid saturation of 0.02 (neutron log data indicate that residual saturation can vary from 0.02 to 0.2). Applying this accounting to the interpolated measured temperature again at two years of heating showed the energy distribution as follows: 77% for heating rock, 12% for heating water, and 11% for vaporizing water. Therefore, global accounting using either simulated temperature and saturation or measured temperatures yields similar results.

3.2.5.5. Water Balance

Since the numerical model explicitly calculates the liquid saturation at every gridblock, the total volume of vaporized water and the total volume of condensed water can be determined from the numerical model output. The difference of the two would be the moisture lost through vapor transport out of the bulkhead. As mass and energy balance is strictly adhered to in the numerical model, this number also equals the model output of the mass loss through the bulkhead (plus very little through the drift walls of the Observation Drift). Numerical-model results show that for the vapor generated, typically twice as much of it escapes through the bulkhead than condenses in the cooler rocks. That is, two thirds of the vaporized water appears to have been lost from the test via transport through the bulkhead. The water balance results indicate that if the DST was a totally closed system, then the zones of increased liquid saturation in the test block would contain possibly three times the current volume of water. The larger volume of water would translate to both an increase in the liquid saturation value in each gridblock, and an increase in the number of gridblocks that have liquid saturation raised above the pre-heat values.

3.2.5.6. Uncertainty in Fate of Thermally Mobilized Water

The condensed water from the vapor that is not lost through the bulkhead is redistributed in the rock mass. Presently, zones of increased and decreased water content (from pre-heat baseline) are being monitored in the DST by periodic geophysical methods and air-permeability measurements. These methods are useful for assessing qualitative changes, but do not give direct and reliable measured value of the absolute liquid saturation/moisture content of the matrix and fractures. In addition, the trends in the data for particular locations in the test are the most useful observations for validating the conceptual processes that control this moisture distribution. The electrical resistivity tomography (ERT), crosshole radar tomography (GPR) and neutron log data are used to validate the process models in the following manner. Simulated matrix liquid saturation contours at different phases of heating are generated in the appropriate planes of geophysical measurements. Zones of drying and wetting from the ERT and GPR tomograms at specific times of measurements are compared to the simulated contours of liquid saturation. Since neutron logging data are point measurements, locations of drying with time of heating as logged are compared to the progression of the drying front in the simulated liquid saturation. The thermal test team has made animations of both simulation and measurements to show they track each other closely.

While the geophysical measurements monitor mostly the water content changes in the matrix (the matrix porosity is at least an order of magnitude larger than the fracture porosity), periodic air injection tests are performed in the twelve hydrology boreholes to assess primarily the wetting and drying in the fractures. These measurements may also reflect any thermal mechanical and/or coupled hydrochemical processes that change fracture permeability (these latter effects are anticipated to be small compared to the thermal-hydrological effects in those zones of increased saturation). Wetting of fractures means increase resistance to air flow during air-injection tests, leading to a decrease in air

permeability from its pre-heat value. These permeability data are used to validate the process model in the following manner. Simulated fracture liquid saturation contours at different phases of heating are generated in the planes of the 12 hydrology boreholes. Then the measured permeability values are compiled and correlated to the simulated fracture saturations. To do this, the measurements are taken quarterly in different borehole sections, with each normalized to its pre-heat value. It is observed that for those borehole sections situated in zones of increased liquid saturation as predicted by the numerical model, the measurements display a trend of decrease in permeability. As heating progresses and the drying around the Heated Drift and the wing heaters expands, certain borehole sections that were previously zones of increased liquid saturation would become zones of decreased (simulated) liquid saturation. Indeed, the measured permeability in some borehole sections below the wing heaters that have shown the largest decrease in permeability very early in the heating phase are observed to return later in the heating phase to their pre-heat levels.

It is evident from the discussion above that measurements for monitoring moisture redistribution in the DST are by nature indirect and qualitative. Nonetheless, locations of dry-out and condensation deduced from ERT, GPR, neutron logs and air permeability in general corroborate well with the simulated time evolution of the liquid-saturation changes in the matrix and fractures. This indicates that the modeling has captured the fate of the thermally mobilized water for the open-system DST, given the inherent uncertainty of the measurements. Were the DST an ideally closed system with no vapor loss through the bulkhead, the total volume of redistributed condensed water in the test block may be several times higher. The larger volume of condensate would perhaps promote more drainage down the fractures and cause more wetting below than above the heated horizon.

Although a closed boundary condition on the bulkhead to simulate a closed-system can be implemented, the geophysical methods do not discriminate as precisely as the models between the differences of moisture redistribution of the two cases: open and closed systems. Conversely, if the actual amount of vapor loss through the bulkhead were much larger than the range calculated, the wetting will be less, and it is not certain whether the geophysical methods can discriminate the different degree of wetting unless there was a qualitative change in the distribution. Therefore, the geophysical measurements are valuable for validating the thermal hydrological processes of boiling, drying, and condensation in the numerical models, but they are not that useful for differentiating the subtle differences of different degrees of wetting from alternative conceptual models. In this context, a direct measurement of heat/mass loss through the bulkhead would have little impact on the understanding and usage of the thermal-hydrological measurements and observations from the DST

3.2.5.7. Conclusions Drawn from the DST

Discussions in the previous sub-sections demonstrate the DOE's understanding of the fundamental thermal-hydrological processes in the DST, including the mass and energy loss through the bulkhead. The favorable comparison of the DST calculated and

measured temperatures, and the corroboration of the calculated moisture redistribution and moisture measurements, indicate that the relevant thermal-hydrological processes are adequately addressed in the TH process models. Therefore the objectives of acquiring a more in-depth understanding of the coupled processes and validating the conceptual thermohydrologic processes at a drift scale are being met in the DST. Because of the DST, there is increased confidence in the prediction of repository performance when these same numerical models are applied to systems with different boundary conditions, different thermal loading, and different time-scale.

However, it should be emphasized that the measurements in the DST are not being applied directly to address performance issues. For example, the reduced volume of condensed water in the open-system (compared to that of an ideally closed system) can reduce the potential of seepage into the drift. Thus, it would not be appropriate to conclude that water will not seep into the potential emplacement drifts, because the DST remote camera has not shown water dripping into the Heated Drift. On the other hand, the DST has given the DOE confidence that important components of TH processes have not been omitted in the TH process models. These same process models can be, and have been, applied to actual repository conditions (heat load and spatial heterogeneity). If TH process models of anticipated repository conditions indicate seepage does not occur into the emplacement drifts, then the results are credible because the TH process models have been validated using DST measurements of thermal-hydrological responses.

Similarly, because of the smaller volume of condensed water in the open-system DST, the hydrological observations of possible fluid movement during the cool down phase of the DST may differ from that of a closed-system. Therefore, caution must be exercised not to directly apply the results of DST to performance issues. Rather, the increased understanding of coupled process behavior should be indirectly applied to performance issues through abstraction of observations and results.

3.2.6. References

Buscheck, T.A., and J.J. Nitao 1995, *Thermal-hydrological Analysis of Large-Scale Thermal Tests in the Exploratory Studies Facility at Yucca Mountain*, UCRL_ID-121791, Livermore, CA: Lawrence Livermore National Laboratory.

CRWMS M&O 1996. *Test Design, Plans, and Layout for the ESF Thermal Test*, BAB000000-01717-4600-00025-REV 01, Contract Number DE-AC01-91RW00134, September.

CRWMS M&O 1998a. *Drift Scale Test As-Built Report*, BAB000000-01717-5700-00003-REV 01, Contract Number DE-AC08-91RW00134, September.

CRWMS M&O 1998b *Thermal Test Informal Progress Report No. 1*, Las Vegas, NV, December.

CRWMS M&O 1999a *DOE/NRC Appendix 7 Meeting on Thermal Testing, Las Vegas, April 28, 1999.*

CRWMS M&O 1999b *Thermal Test Informal Progress Report No. 2,* Las Vegas, NV, April.

CRWMS M&O 1999c. *Thermal Test Informal Progress Report No. 3,* Las Vegas, NV, July.

CRWMS M&O 2000, *Cross-Drift Thermal Test Planning Report,* Las Vegas, NV, August.

CRWMS M&O 2001a, *Thermal Test Informal Progress Report No. 6,* Las Vegas, NV, April.

CRWMS M&O 2001b, *Meeting Summary, NRC/DOE Technical Exchange on Thermal Effects on Flow Key Technical Issue, January 8-9, 2001, YMP e-mail sent by Veronica Cornell, January 22, 2001*

Datta, R.N. 1998, *Movement of Moisture Through Drift Scale Test Bulkhead,* YMP e-mail circulated May 5, 1998, Las Vegas, NV

DOE 2000, U.S. DOE Review of the NRC's Thermal Effects on Flow Issue Resolution Status Report, Revision 2, letter from Stephan Brocoum to C. William Reamer, March 22, 2000.

Nuclear Regulatory Commission 1999, *Issue Resolution Status Report: Key Technical Issue – Thermal Effects on Flow - Revision 2,* Division of Waste Management, Office of Nuclear Material Safety and Safeguards, August.

Nuclear Regulatory Commission 2000, *Issue Resolution Status Report: Key Technical Issue – Thermal Effects on Flow - Revision 3,* Division of Waste Management, Office of Nuclear Material Safety and Safeguards, November.

Wagner, R.A. 1999, *Assessment of Heat Loss Through the Drift Scale Test Bulkhead,* Interoffice Correspondence, October 21, 1999, Las Vegas, NV

3.3 Bulkhead Vapor and Heat Loss Measurements Preliminary Results

This draft report summarizes the approach and preliminary findings to determine the mass and heat loss from the Heated Drift bulkhead. The basic approach involves measuring the temperature, T, and the relative humidity, R_H, on the cool side of the Heated Drift, as a function of time and discrete spatial locations. The measured T and R_H are subsequently used to calculate the changes in vapor mass and energy during normal operating conditions and perturbed conditions. Here, normal conditions means when the vent lines are open and air is blown at the bulkhead at ~21,000 cfm. Disturbed conditions refer to when the airflow is shut off and/or reduced. The latter conditions comprise the main measurement events.

3.3.1 Temperature and Relative Humidity Measurements

Sensors' Placement A total of 38 Rotronic HygroClip® relative humidity - temperature sensors were installed in two rows of sensors in the x-direction (see the conceptual drawing as well as the number used to refer to each sensor in Figure 14). Each row (i.e., the left and center rows) were respectively comprised of six and seven columns of sensors in the y-direction. Each column were ~3 (ft) apart, with the first column being ~3 (ft) away from the bulkhead (see also Figure 14). Additionally, each column included three sensors in the z-direction covering a distance of roughly 11 (ft) from the tunnel ceiling to the floor (see Figure 15). Except the seventh column of the center row (i.e., sensors 19 and 20) included only two sensors. The picture in Figure 16 provides a better depiction of the way the various sensors were installed. Also, note from this figure that the orange colored "streamers" were used to determine the airflow pattern during the measurements.

Measurement Events On July 18th and 19th, 2001 three separate sets of measurements were conducted, where during each event the main airflow through the ductwork in the tunnel was shut off. The changes in the temperature and relative humidity, as a result of disturbing the normal operating condition, are thought to be directly associated with the heat and moisture loss through the DST bulkhead. Finally, during the various measurement events (i.e., while the airflow was shut off) in order to keep the air as mixed as possible and prevent vapor condensation, a number of 18-inch Hampton Bay® high velocity fans were placed on the floor. The three measurement events can be summarized as follows:

- Measurement Number 1A lasted from 09:11 to 10:43 with the small fans configured such that they were taking air away from the bulkhead
- Measurement Number 1B lasted from 10:43 to 11:32 during which time the small fans were also turned off. From 11:32 to ~12:30 the main air vents were turned back on allowing the system to return back to a normal operating condition
- Measurement Number 2 lasted from 12:30 to 14:15. For this event, the configuration of small fans was changed such that four fans were placed on the platform near the bulkhead. Four other fans were placed ~18 ft. away from the bulkhead as an attempt to uniformly pull the hotter air away from the bulkhead.
- Measurement Number 3 lasted from 09:16 to 11:12 on 7/19/2001. For this event a plastic curtain was placed ~18 ft. away from the bulkhead. In addition, ten fans were

placed on the floor, blowing upward towards the ceiling. At 11:12 the curtain was removed, however, the fans were kept on with the main air vents shut off for another 24 minutes.

It must be noted that, even though an attempt was made to place the small fans such that the mixing is uniform as possible, the movement of orange streamers were fairly erratic for the most part. That is, the small fans resulted in turbulent mixing of the moist air.

Measured Temperature and Humidity Histories Time histories for the measured temperature and relative humidity during the three different events are respectively shown in Figures 17 and 18. For clarity, each row is divided to three planes representing the top (i.e., near the ceiling), middle, and bottom (i.e., near the floor) sensors. The time histories are then plotted for each column starting from the sensor closest to the bulkhead. In these figures, each data set is presented without smoothing. However, if for any pair of data points a negative T and/or negative R_H values were recorded, that pair of data was simply ignored.

As Figure 17 shows, during the first measurement event, the largest temperature rise occurs near the ceiling for the sensors closest to the bulkhead (i.e., no. 36). Naturally, there are smaller rises in the temperature for the sensors further away from the bulkhead and/or are located at the middle and bottom planes. This illustrates the greatest gradients are at the top (i.e., near the ceiling). It is interesting that, sensor no. 1, which is located in the same y and z locations as no. 36, does not experience a similar dramatic rise as that of no. 36. This may reflect a problem with sensor 36, be an artifact of poor air mixing during the measurement event, or may even be a correct response since the air warmest and driest there. To better assess this response of sensor no. 36, the long-term data that has been continuously collected for the past five weeks must be analyzed. Yet another interesting feature of the temperature histories is, during the measurement 1B (i.e., when both the air vents and small fans are shut off) while the upper portions (with the exception of no. 36) continue to experience a rise in the temperature, the lower planes quickly cool off. This is indicative of the cooler air being pulled from connecting drift that is being warmed up as it rises.

In Figure 18, the relative humidity temporal variations illustrate the R_H decreases when there is sudden increase in the temperature. However, it is interesting that when the temperature suddenly rises, the humidity also initially increases and then R_H decreases as T continues to rise. The initial simultaneous rise in R_H and T is indicative of a sudden increase in the vapor content. Additionally, the wavy nature of the R_H histories, in particular during the normal operating conditions, depicts the effect of daily variations in the barometric pressure. An interesting feature of the R_H response, during the normal operating conditions, is that the traces for the various sensors are quite distinct. That is, even though the sensors in the y-direction are ~3 ft. apart there is a gradient in the R_H and thus, vapor mass.

3.3.2 Vapor Mass and Energy Calculations

Since the only measured properties include the temperature and relative humidity associated with the vapor flow, other quantities, such as the vapor mass and energy must

be evaluated from the measured values. To calculate the amount of vapor mass corresponding to each sensor, we simply let:

$$m_v(s;t) = \rho_v(s;t)\,\Delta V_s \tag{1}$$

where $m_v(s;t)$ and $\rho_v(s;t)$ refer to the vapor mass and density for each sensor, s, and time, t, and ΔV_s is an assumed control volume for each sensor (see Table 1 for a list of values). In general, vapor density is a function of the vapor pressure, P_v and the measured temperature, T. For instance, using the ideal gas law we can write:

$$\rho_v(s;t) = \left(\frac{M_v}{R}\right)\frac{P_v(s;t)}{T(s;t)} \tag{2}$$

where M_v and R are the molecular weight and universal gas constant, respectively. Vapor pressure, P_v, can be found as a function of R_H and saturation pressure [*Sonntag and Van Wylen*, 1982]:

$$P_v(s;t) = R_H(s;t)\,P_g(s;t) \tag{3}$$

where P_g, is the saturated gas pressure at temperature, T, and is found from the steam tables [e.g., *Harvey et al.*, 2000]. Alternatively, vapor density can be directly evaluated from NIST/ASME Steam Properties [*Harvey et al.*, 2000]. We compared the calculated ρ_v using both the ideal gas law and steam properties and found the absolute difference between the two methods, for most cases is less than 10^{-4} (kg/m^3).

The energy associated with the vapor leaving the DST bulkhead is a function of vapor mass and the enthalpy of vaporization as:

$$E_v(s;t) = h_{fg}(s;t)\,m_v(s;t) \tag{4}$$

where E_v is the vapor energy, h_{fg} is the enthalpy of vaporization and is determined as the difference between the enthalpies of the saturated liquid, h_f, and vapor, h_g [*Sonntag and Van Wylen*, 1982]. The values for h_f and h_g are obtained using the steam properties [e.g., *Harvey et al.*, 2000].

3.3.3 Calculations of Total Increases in Vapor Mass and Energy

In order to determine the change in the vapor mass and energy (i.e., the differences between the normal operating conditions and when the airflow into the drift is reduce and/or stopped), we can simply write:

$$\Delta m_v(s;t) = m_v(s;t) - m_v(s;t_{ref}) \tag{5a}$$

$$\Delta E_v(s;t) = E_v(s;t) - E_v(s;t_{ref}) \tag{5b}$$

where Δm_v and ΔE_v represent the change in vapor mass and energy, respectively, and t_{ref} is a known reference time (e.g., the time before disturbing the normal operating condition). By summing the various Δm_v and ΔE_v values over all sensors locations, we can then determine the net increase in the vapor mass and energy, within the measurement volume, as a function of time, or:

$$m_{v,tot}(t) = \sum_s \Delta m_v(s;t) \tag{6a}$$

$$E_{v,tot}(t) = \sum_s \Delta E_v(s;t) \tag{6b}$$

where $m_{v,tot}$ and $E_{v,tot}$ are the net total vapor mass and energy values as a function of time.

3.3.4 Preliminary Results

Here, we focus our analysis on the first measurement event. That is, we consider the T and R_H temporal variations over a time span of approximately 1.5 hours, and try to calculate the quantity of moisture and heat loss from the bulkhead during this time period. Clearly, the same procedure can be extended to the other two measurement events.

Calculated Vapor Mass and Energy Histories Figures 19 and 20 show the calculated vapor mass and energy histories, respectively evaluated using (1) and (4), for the first measurement event. Comparing these figures to the corresponding time in Figures 17 and 18, when T and R_H first rise, there are also increases in the vapor mass and energy. It appears that, both vapor mass and energy histories, however, display a "pseudo-steady" behavior. That is, even though the temperature continues to rise (e.g., compare Figures 17 with Figures 19 and/or 20) mass and energy in average yield a steady response. We can then take advantage of this response of the mass and determine the net total increase in the energy and thus the heat loss from the bulkhead.

Calculated Total Vapor and Heat Loss The net total vapor mass and heat loss during the first 1.5 hours of the measurement number 1A are respectively shown in Figures 21 and 22. In these figures, we have used (6a) and (6b) to respectively find the total mass and energy. To calculate the net m_v and E_v as a function of time, we consider a reference time of t_{ref}=15 hours as the initial condition. As both figures illustrate, the net total vapor mass and energy sharply increase during the first 15 minutes and eventually attain a maximum value at ~24 minutes after the event begins. Using these figures, we let the maximum vapor mass and energy values, respectively, be 0.26 kg at t=15.65 hrs and 626.0 kJ at t=15.55. We also select the minimum mass and energy to be respectively 0.009 kg and 21.35 kJ, both at t=15.2 hrs. Thus, we yield a vapor mass flow rate of ~1.5E-4 kg/s and a total heat loss of ~0.5 kW from the bulkhead. A total heat loss of ~0.5 kW is ~98% lower than what has been predicted by numerical simulations (e.g., see Memo data 5/20/1999 by Barry Freifeld). In his calculations, Freifeld assumes a total volume of ~332 m^3. Considering this value as the total volume and distributing it equally among the 38 sensors, we found the total heat loss becomes ~2.6 kW. That is, if we are

underestimating the total volume by roughly one third, we would still be ~88% below a predicted heat loss of 22 kW.

Typical Vapor Energy Profiles To illustrate the spatial variations of the vapor energy at various sensor locations, Figures 23 depict typical energy profiles in the y-direction (i.e., at distance away from the bulkhead) at t_{ref}=15 hours, at the time when a maximum vapor mass is detected, and the net energy (i.e., the difference between the maximum and t_{ref}=15 hours values). As Figure 23a shows, there is little to no gradient in the y-direction, before the onset of the first measurement event. Note that, the noticeable gradient in the z-direction (i.e., among the top, middle, and bottom planes) is an artifact of the way individual ΔV_s values are chosen. Yet, we can see a clear gradient in the y-direction for the top and middle sensors located at the center row of sensors (see Figure 23b). This is also reflected in the net energy profiles (Figure 23c), even though for these cases there is less of variation from top to bottom.

3.3.5 Recommendations and Planned Future Measurements

The full details of this section will be provided later. However, these preliminary measurements illustrate the need, complications, as well as uncertainty associated with the head and mass loss from the bulkhead. To ensure whether the calculated heat loss value, reported above, is a true measure of the heat loss from the bulkhead, additional measurements are required. For instance, Freifeld in his 1999 memo assumes the vapor leaving the bulkhead is at 100 °C. To attain such a high temperature, we must better confine the vapor existing the bulkhead.

3.3.6 References

Harvey, A. H., A. P. Peskin, and S. A. Klein, NIST/ASME Steam Properties, Users' Guide, Version 2.2, *U.S. Department of Commerce*, NIST, 2000.

Sonntag, R. E. and G. Van Wylen, *Introduction to Thermodynamics Classical and Statistical*, John Wiley & Sons, Inc., USA, 1982.

Table 1. Assumed control volume values assigned to each sensor. The total measurement volume is assumed to a rectangular box (i.e., the curvature of the ceiling is neglected). Each sensor is considered to be at the center of a smaller box of size, ΔV_s.

Sensor No.	Δx_s (m)	Δy_s (m)	Δz_s (m)	$\Delta V_s = \Delta x_s \Delta y_s \Delta z_s$ (m^3)
1, 4, 7, 10, 13, 16	1.69	0.9144	0.61	0.94
2, 5, 8, 11, 14, 17	1.69	0.9144	2.13	3.29
3, 6, 9, 12, 15, 18	1.69	0.9144	0.61	0.94
19, 20	4.72	0.9144	1.68	7.25
21, 24, 27, 30, 33, 36	3.04	0.9144	0.61	1.70
22, 25, 28, 31, 34, 37	3.04	0.9144	2.13	5.92
23, 26, 29, 32, 35, 38	3.04	0.9144	0.61	1.70

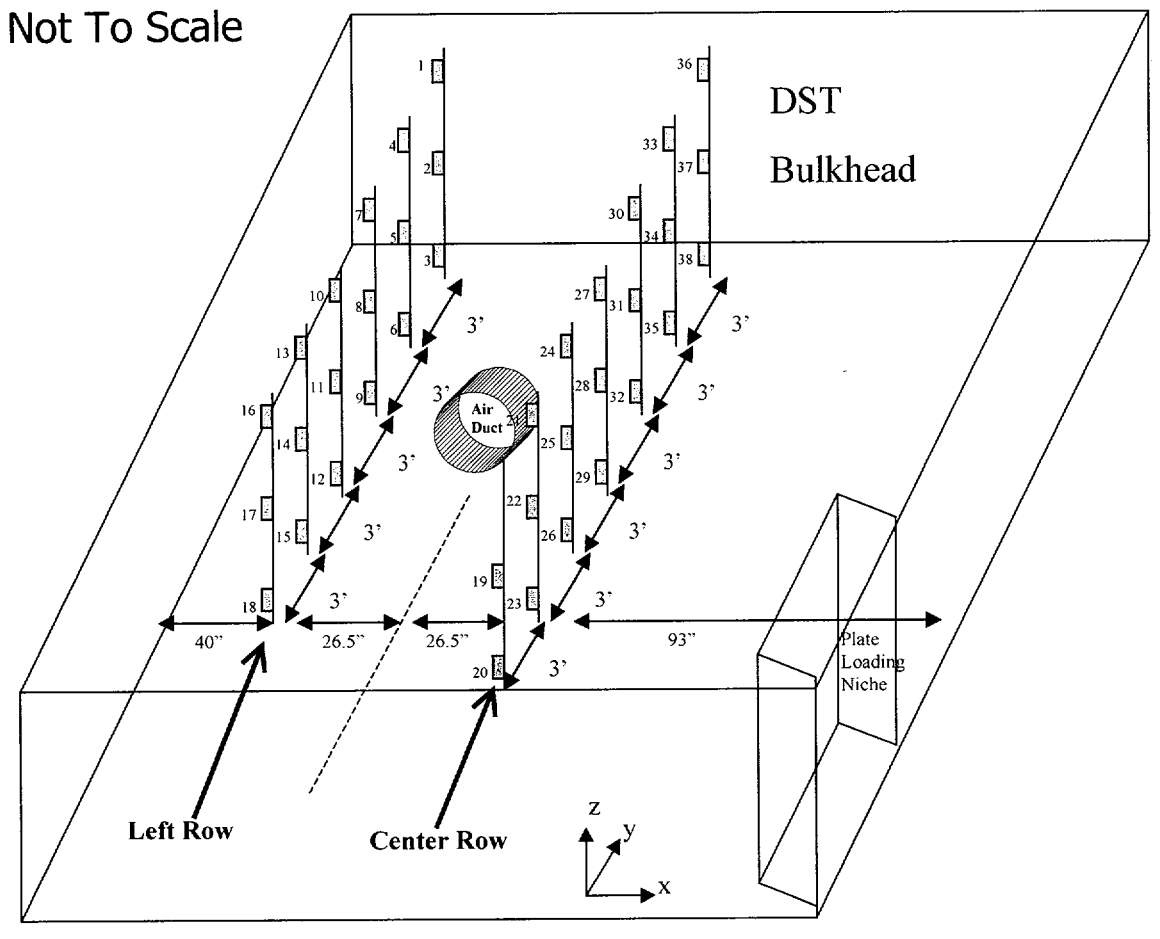

Figure 14. Conceptual Drawing Illustrating the Arrangement of Sensors.

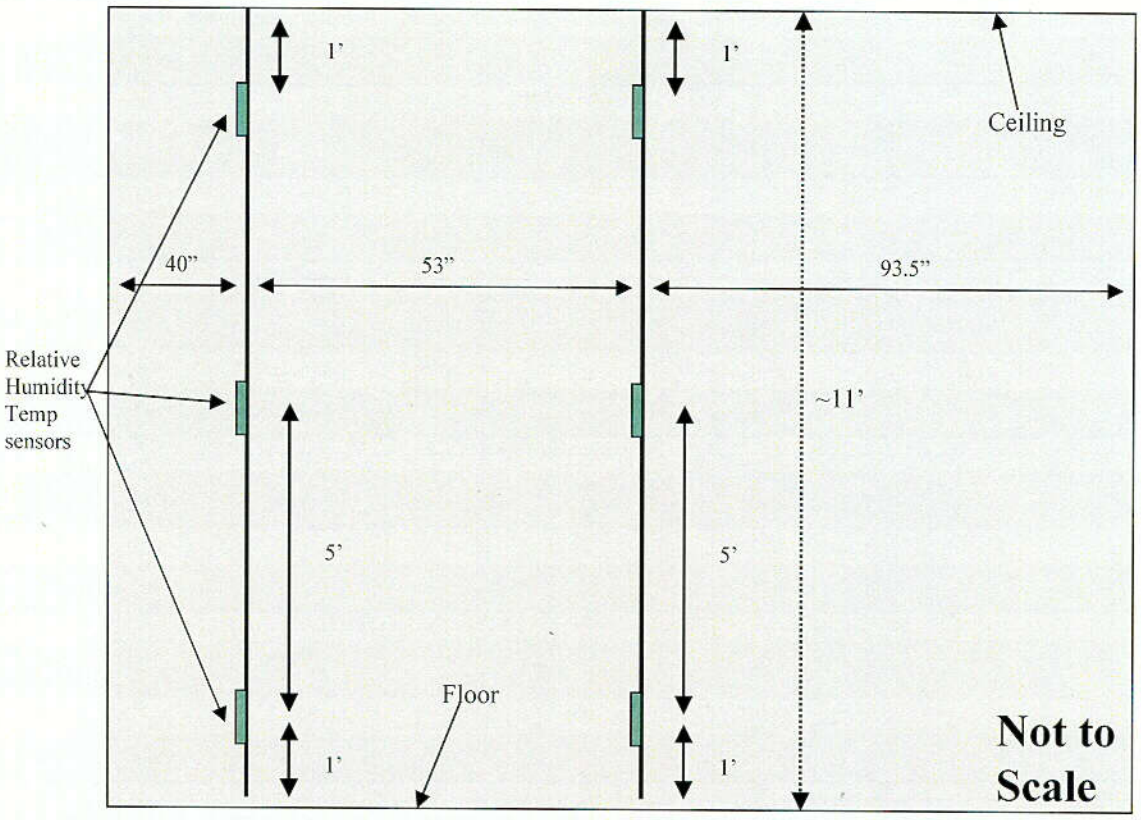

Figure 15. Schematic Sketch of Sensors' Location with Respect to Ceiling and Floor

Figure 16. Photograph of Sensor Positions with Indicator Streamers

C13

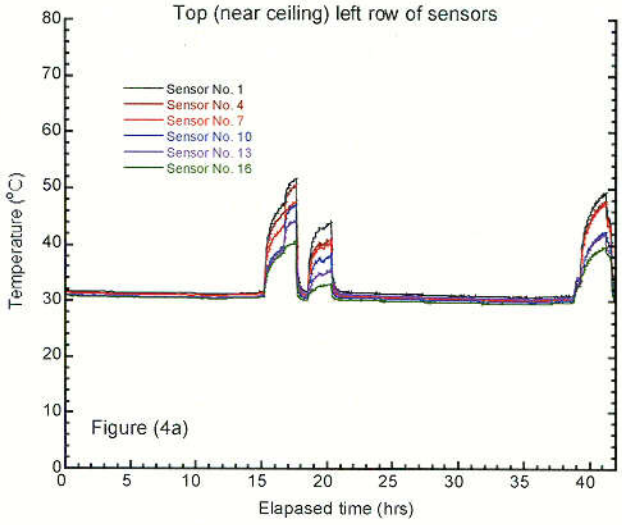

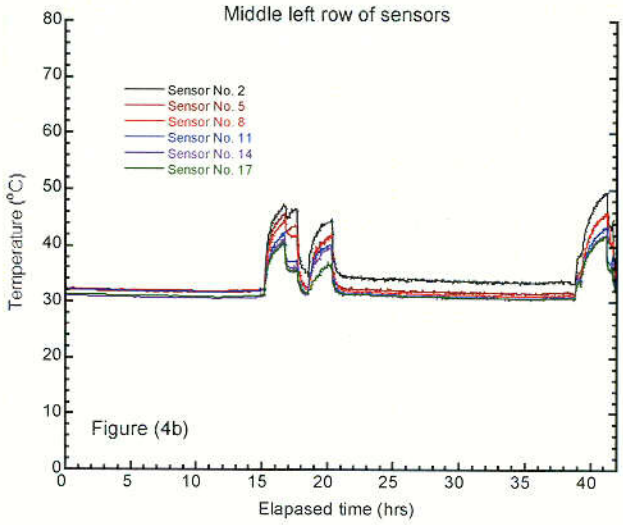

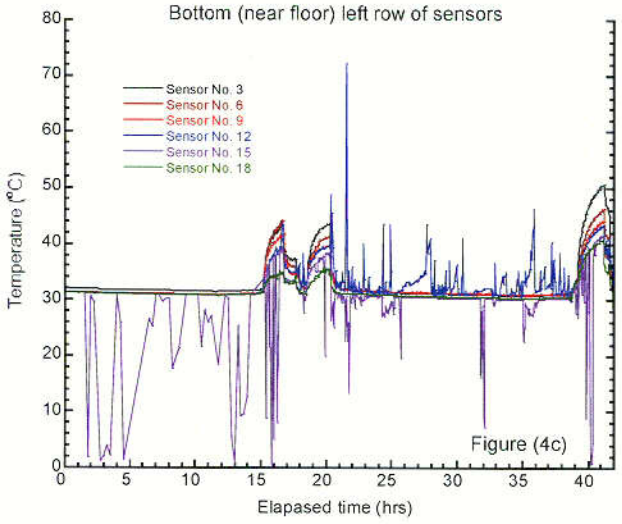

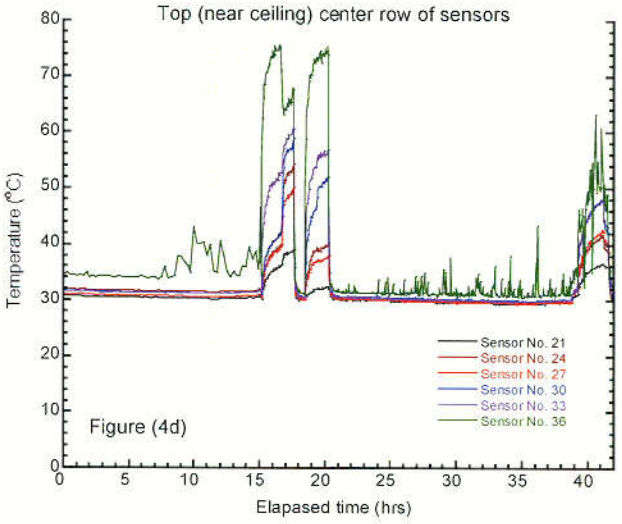

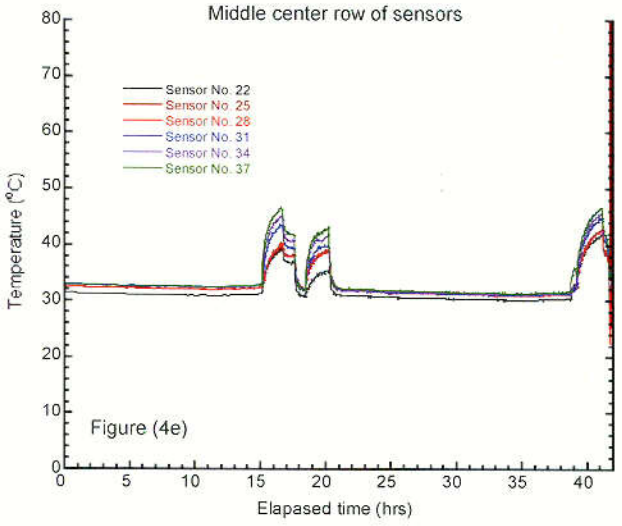

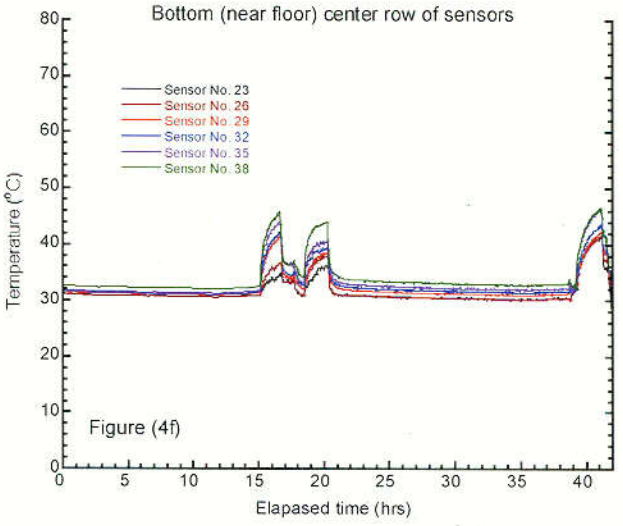

Figure 17. Measured Temperature Time Histories for the Three Measurement Events

C14

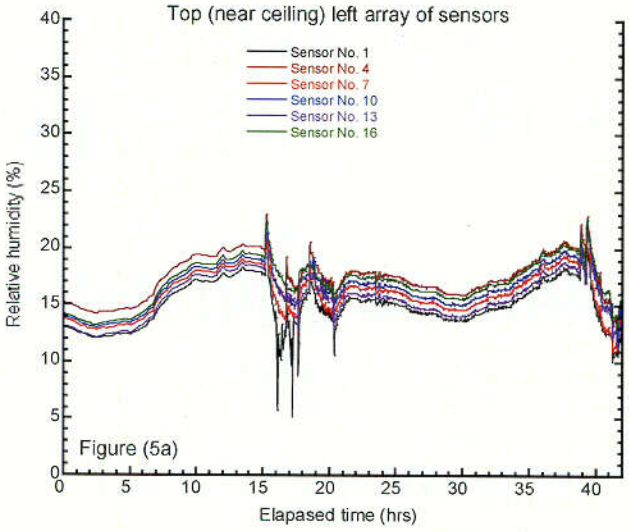

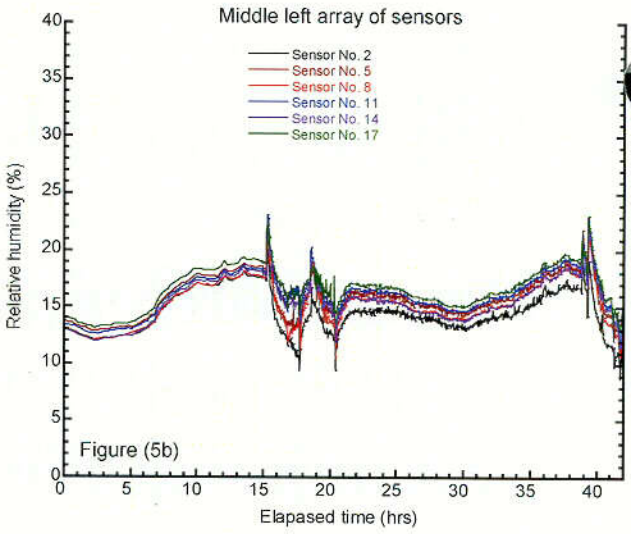

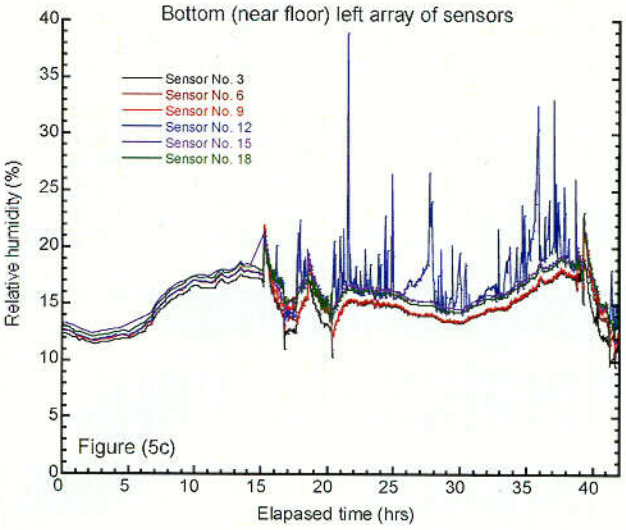

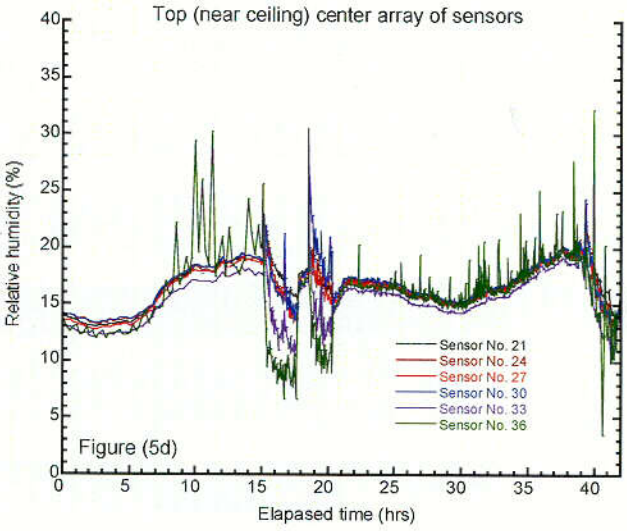

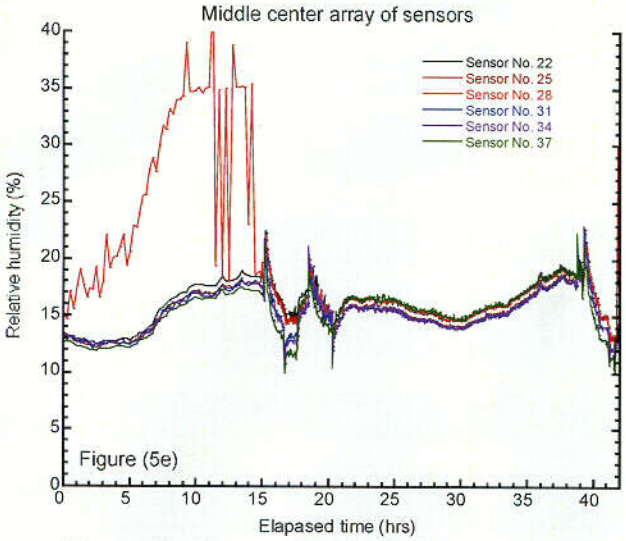

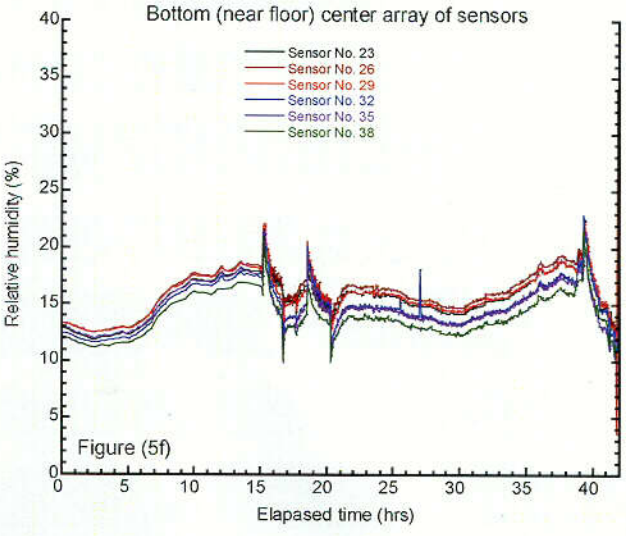

Figure 18. Measured Relative Humidity Time Histories for the Three Measurement Events

C15

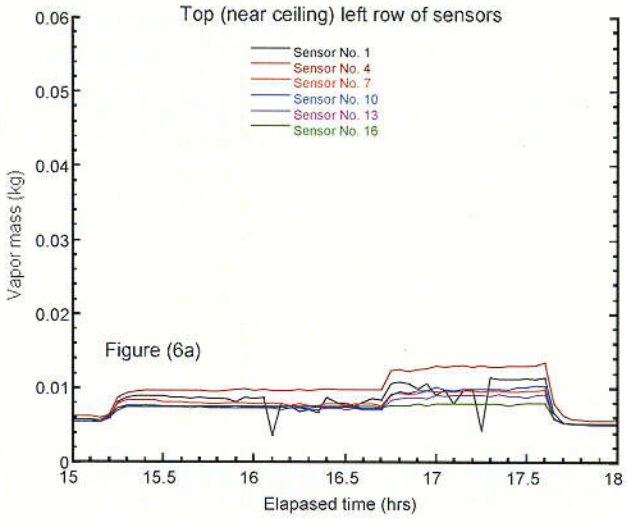

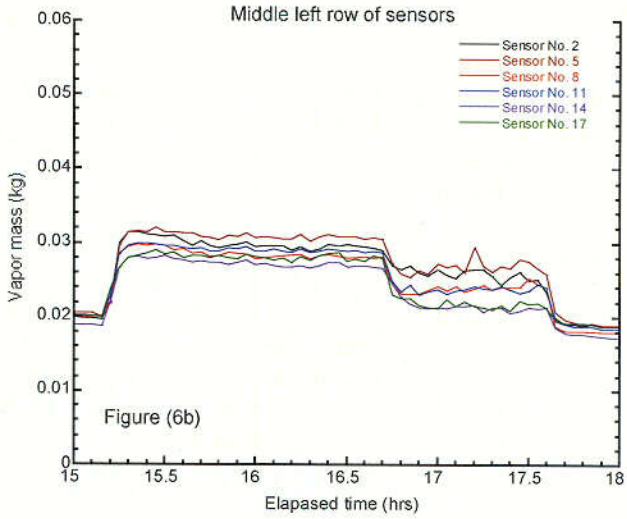

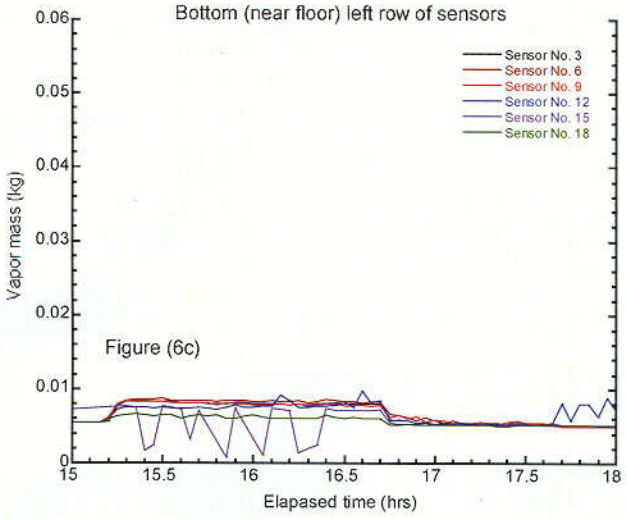

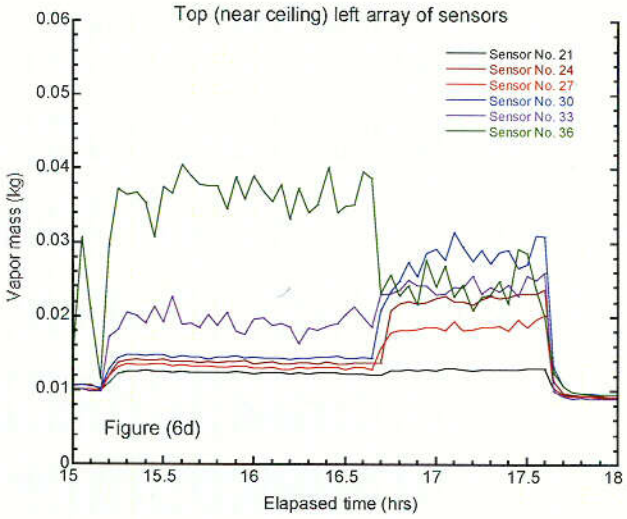

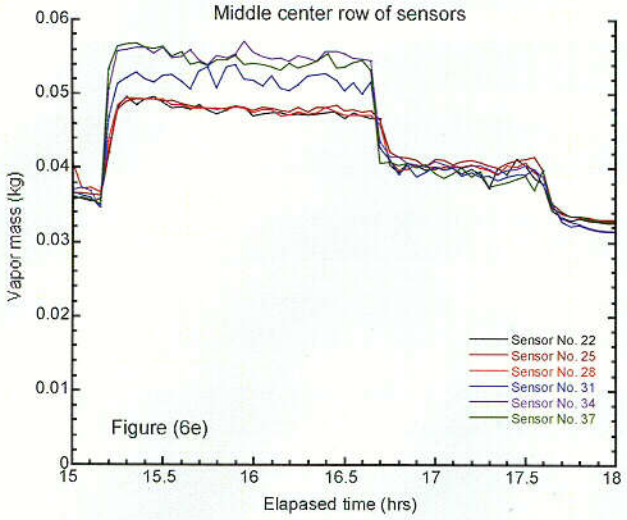

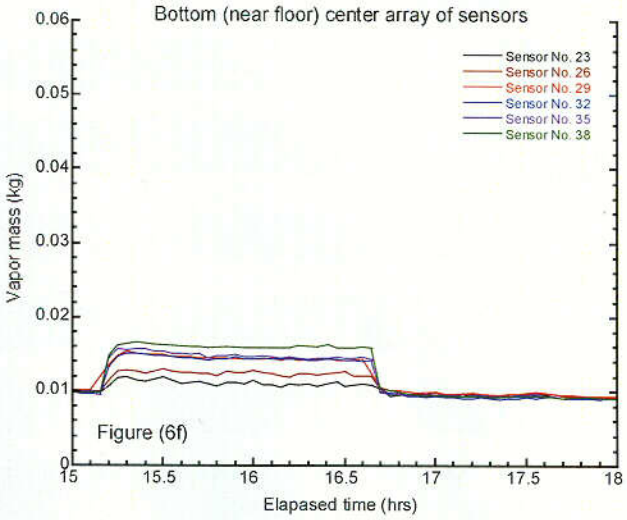

Figure 19. Calculated Vapor Mass Time Histories for the First Measurements Event.

C16

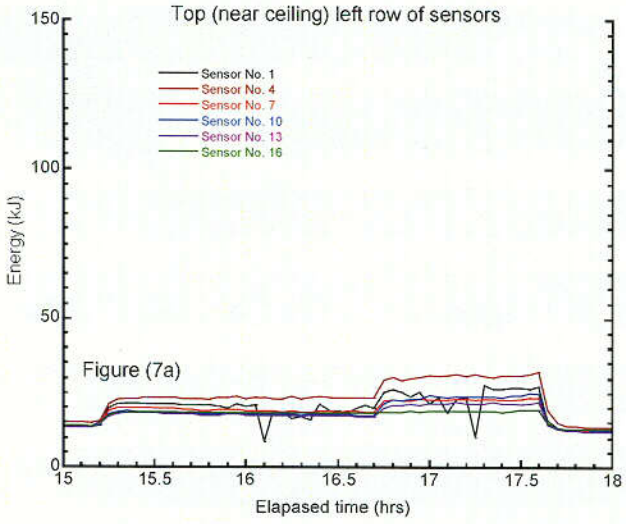

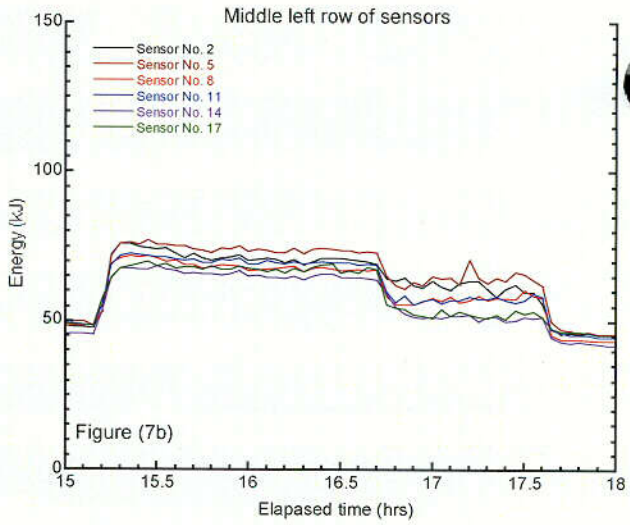

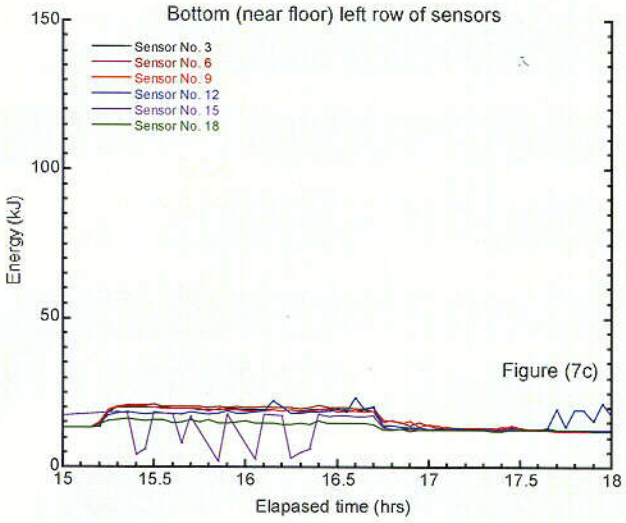

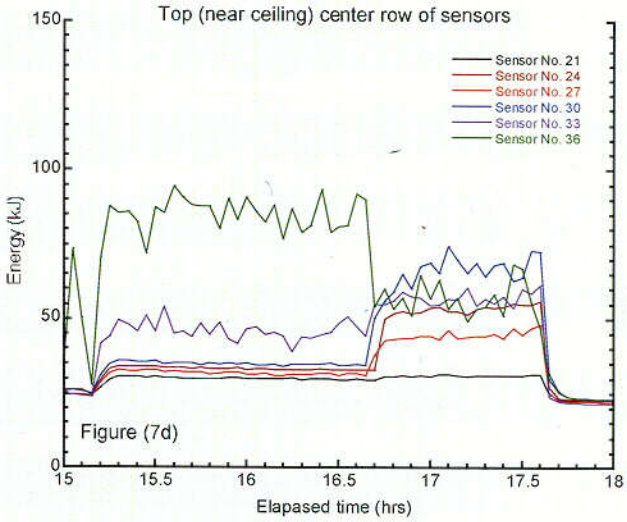

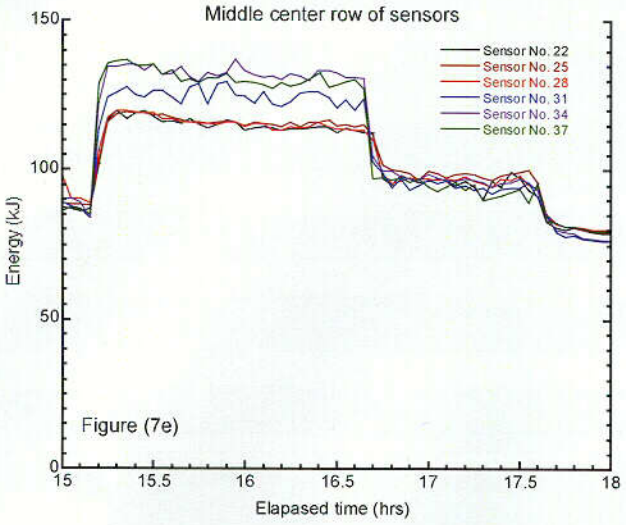

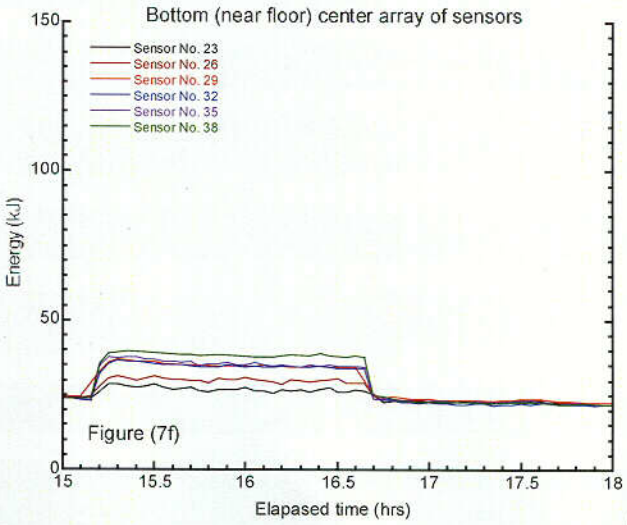

Figure 20. Calculated Vapor Energy Time Histories for the First Measurement Event

C17

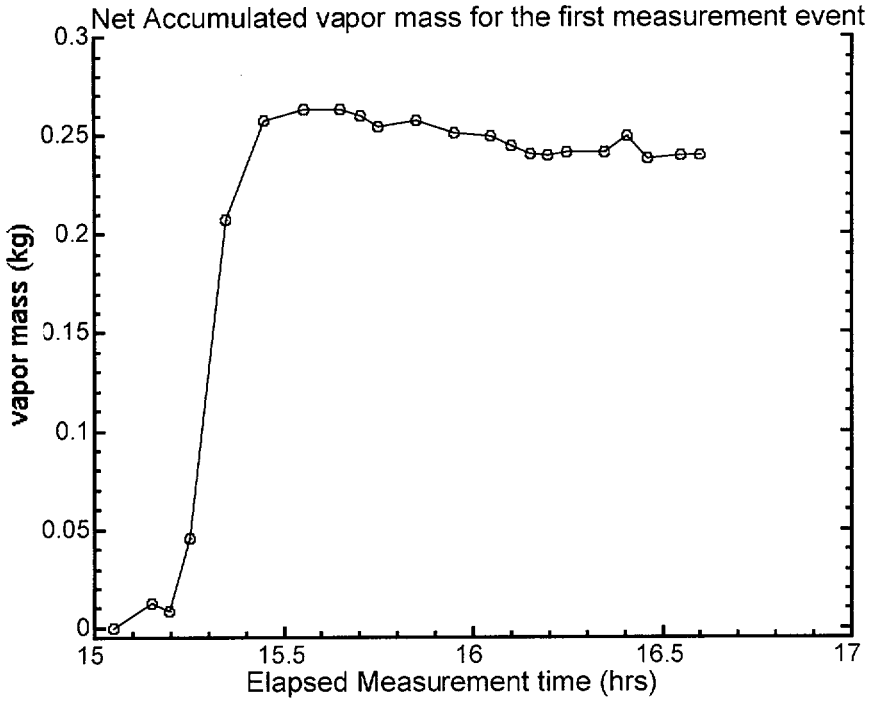

Figure 21. Net Total Vapor Mass as a Function of Time for Measurement number 1A.

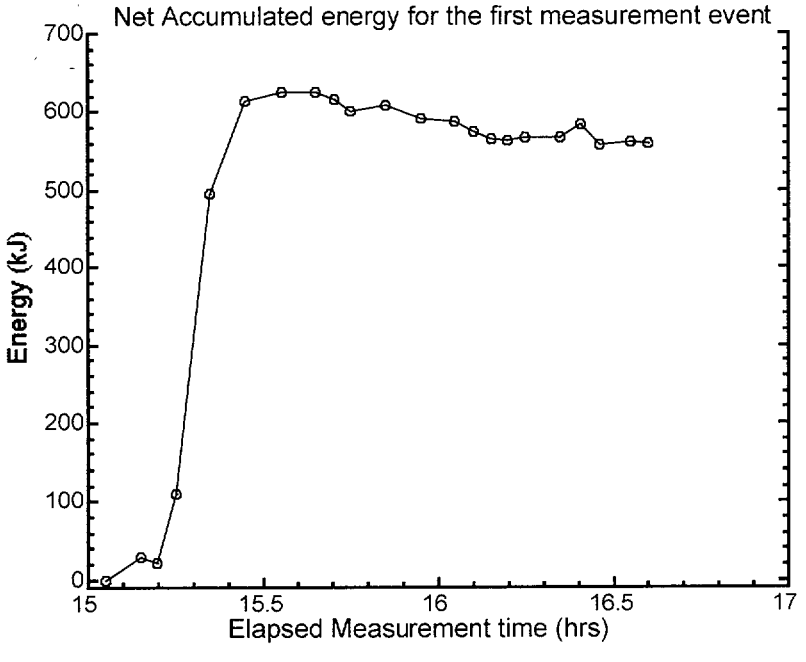

Figure 22. Net Total Vapor Energy as a Function of Time for Measurement Number 1A.

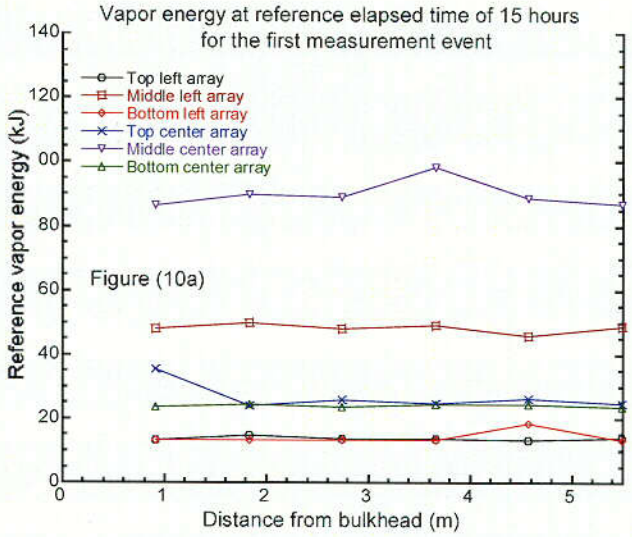

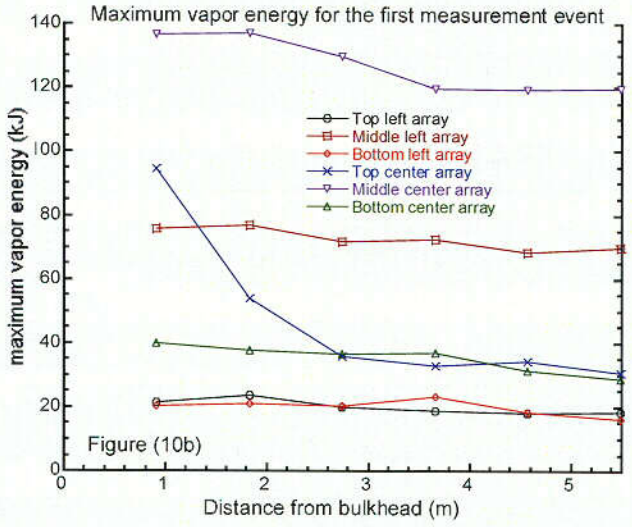

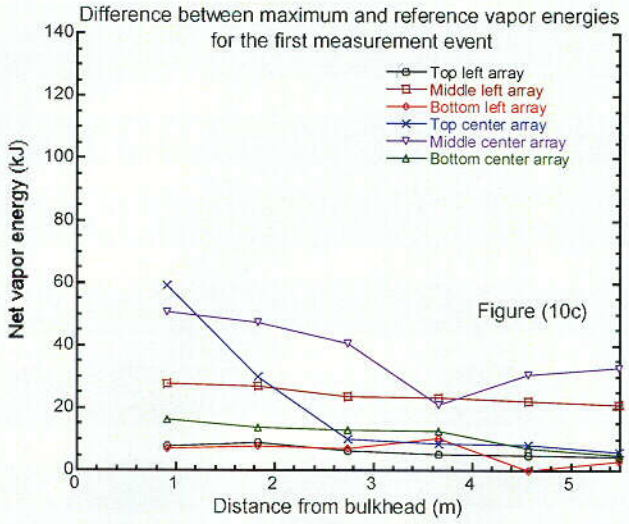

Figure 23. Vapor energy profiles at a reference time of 15 hours, at maximum vapor mass, and net vapor energy at various sensors' locations.

C18